nature communications

Article

https://doi.org/10.1038/s41467-024-54653-9

Xenogeneic-free culture of human intestinal stem cells on functional polymer-coated substrates for scalable, clinical-grade stem cell therapy

Received: 6 March 2024

Accepted: 18 November 2024

Published online: 02 December 2024

Check for updates

Seonghyeon Park[1,13], Ohman Kwon[2,12,13], Hana Lee[2,13], Younghak Cho[1], Jemin Yeun[1], Sung Hyun Yoon[1], Sang Yu Sun[1], Yubin Huh[2,3], Won Dong Yu[2,3], Sohee Park[2,3], Naeun Son[2,3], Sojeong Jeon[2,3], Sugi Lee[4], Dae-Soo Kim[3,4], Sun Young Lee[5], Jin Gyeong Son[5], Kyung Jin Lee[6], Yong Il Kim[6], Jin Hong Lim[7], Jongman Yoo[6,8,9], Tae Geol Lee[5], Mi-Young Son[2,3,8,10] ✉ & Sung Gap Im[1,11] ✉

The need for basement membrane extract (BME) with undefined constituents, such as Matrigel, for intestinal stem cell (ISC) culture in traditional systems poses a significant barrier that must be overcome for the development of clinical-grade, scalable, ready-to-use ISCs. Here, we propose a functional polymer-based xenogeneic-free dish for the culture of intestinal stem cells (XF-DISC), ensuring substantially prolonged maintenance of ISCs derived from 3-dimensional human intestinal organoids ($ISCs^{3D\text{-}hIO}$). XF-DISC enables remarkable expandability, exhibiting a 24-fold increase in cell numbers within 30 days, with long-term maintenance of $ISCs^{3D\text{-}hIO}$ for more than 30 consecutive passages (>210 days). In addition, XF-DISC is fully compatible with a cell banking system. Notably, human pluripotent stem cell-derived $ISCs^{3D\text{-}hIO}$ cultured on XF-DISC are successfully transplanted into intestinal injury and inflammation mouse models, leading to engraftment and regeneration of damaged mouse intestinal epithelium. As a reliable and scalable xenogeneic-free $ISC^{3D\text{-}hIO}$ culture method, XF-DISC is highly promising for the development of regenerative ISC therapy for human intestinal diseases.

Inflammatory bowel disease (IBD) affects many individuals, causing significant pain and suffering because of the lack of a complete cure. According to a 2016 Centers for Disease Control and Prevention (CDC) report, 1.3% of U.S. adults were diagnosed with IBD in 2015, highlighting its prevalence and impact on quality of life and health care costs. Additionally, the World Health Organization (WHO) reported a death rate of greater than 75 per 100,000 due to IBD, with older adults, especially women, being more affected. Current treatments, such as anti-TNF-α drugs, offer symptomatic relief but do not address the underlying causes, whereas MSC-based cell therapy provides indirect benefits. Therefore, developing innovative cell therapies is crucial for effective regeneration and advancing treatments for gastrointestinal diseases[1–4].

Intestinal stem cells (ISCs) are self-organizing stem cells capable of forming organoids that resemble their native organ[5–10]. ISCs have garnered considerable interest in the last decade as promising sources for stem cell therapy in regenerative transplantation to treat intestinal diseases[11–15]. Recently, human intestinal organoid (hIO) culture has

A full list of affiliations appears at the end of the paper. ✉e-mail: myson@kribb.re.kr; sgim@kaist.ac.kr

emerged as an exceptional technology for investigating the molecular and cellular nature of ISCs in vitro. However, it remains a challenge to specifically isolate pure ISC populations from hIOs and efficiently enrich ISCs in vitro because only a small portion of ISCs (>1%) occupy hIOs[16].

Previous methods, including our own, commonly require feeder cell layers[17] or basement membrane extracts (BMEs), such as Matrigel[18], for the culture of ISCs$^{3D\text{-}hIO}$. The undefined culture environment associated with the feeder cell layer or BME results in various limitations and raises serious clinical concerns in therapeutic settings[19], including batch-to-batch variation, limited reproducibility, risk of pathogenic transfer, and the presence of nonhuman immunogenic epitopes such as *N*-glycolylneuraminic acid[20]. Consequently, there is an urgent need for the development of alternatives that can accommodate valuable cell sources, such as ISCs$^{3D\text{-}hIO}$, that are compatible with their subsequent clinical applications[21–25]. Such efforts will enable us to establish unique in vitro culturable ISCs$^{3D\text{-}hIO}$ as a source for novel ISC-based remedies, which represent promising therapeutic modalities for refractory intestinal failure.

Alternative substrates that can efficiently assist in xenogeneic-free culture of ISC$^{3D\text{-}hIO}$ should be chemically well-defined and synthetically scalable to ensure reconstruction of the stem cell microenvironment with high reproducibility. Several efforts to establish a xenogeneic-free and chemically defined environment for reliable ISC culture without the use of a feeder cell layer or BME have been ongoing[21,26]. However, despite these efforts, the development of a scalable yet stable clinical-grade ISC culture platform with a facile fabrication process that preserves the great expansion potential of these cells and satisfies the high level of efficacy and safety criteria for the treatment of gastrointestinal disorders falls short of expectations and remains a highly crucial and pressing issue.

Here, we developed a **X**enogeneic-**F**ree **D**ish for **ISC** (XF-DISC) surface using a biocompatible functional polymer coating deposited directly on cell culture substrates via a vapor-phase method, namely, initiated chemical vapor deposition (iCVD). The XF-DISC not only facilitated exceptional scalability with 24-fold increased proliferation in 30 days but also supported 30 transfers every 7-10 days, which is equivalent to more than 210 days. In addition, compared with the same cells cultured on Matrigel-coated surfaces, XF-DISC facilitated stable preservation of ISCs$^{3D\text{-}hIO}$ even after storage for 3 years and enabled efficient differentiation into the intestinal epithelium, with no discernible distinction. Furthermore, ISCs$^{3D\text{-}hIO}$ cultured on XF-DISC were capable of engrafting and regenerating the intestinal epithelium of EDTA-induced injury and dextran sulfate sodium (DSS)-induced colitis disease models via orthologous transplantation. These findings collectively highlight XF-DISC as a promising avenue for harnessing the full potential of the ISC therapeutic strategy in various intestinal syndromes.

Results

Exploration of xenogeneic-free culture surfaces

ISCs$^{3D\text{-}hIO}$ differentiated from human induced pluripotent stem cells (hiPSCs) on Matrigel-coated cell culture surfaces could facilitate massive culture and transplantation[18]. Nonetheless, their potential application as cellular remedies for humans is inherently limited because of concerns regarding acute immune responses in human recipients[27]. The development of an ISC$^{3D\text{-}hIO}$ culture platform without the use of xenogeneic ECM could overcome the intrinsic limitations of cellular treatment. Therefore, we aimed to discover an optimal surface for the xenogeneic-free and highly expandable culture of ISCs$^{3D\text{-}hIO}$ using cell culture surface modifications. Leveraging the benefits of the iCVD process[28], which enables damage-free polymer film synthesis from various monomers, we conducted a comprehensive polymer-based screening (Fig. 1a). In more detail, the iCVD process allows the formation of compositionally uniform copolymers with a systematically controlled composition of each monomer[28–33]. Notably, the vapor phase characteristics enabled the synthesis of copolymers without phase separation, rendering this process optimal for generating diverse types of uniform copolymer compositions. Additionally, the solvent-free and additive-free nature of the process inherently eliminates the issues related to cell toxicity arising from residual solvents or additives[34,35]. The ambient temperature further provided the advantage of coating the polymer film without damaging the conventional cell culture plates[36]. Moreover, conformal thin films can be deposited directly onto nonflat culture surfaces, such as multiwell plates and membrane inserts, while preserving their original forms[37]. The benefits of the iCVD process ensure reproducible and scalable surface modifications of cell culture plates with various form factors. By utilizing such advantageous characteristics, we synthesized diverse types of polymers using the iCVD process, thereby adjusting the possibility of xenogeneic-free culture of ISCs$^{3D\text{-}hIO}$.

In this study, we deposited 32 distinct types of polymers with diverse functional characteristics, such as cationic/anionic functionalities, crosslinking capabilities, and hydrophobic and hydrophilic properties (Fig. 1b). The names, specific synthesis conditions, and Fourier transform infrared spectroscopy (FT-IR) analysis results of each polymer are summarized in Supplementary Fig. 1 and Supplementary Tables 1 and 2. Polymers such as poly(2-(dimethyl amino) ethyl methacrylate) (pDMAEMA), poly(*N*,*N*-dimethyl aminopropyl methacrylamide) (pDMAPMA), poly(2-(diethyl amino) ethyl methacrylate) (pDEAEMA), poly(2-(*tert*-butyl amino) ethyl methacrylate) (pTBAEMA) and poly(2-(dimethyl amino) ethyl acrylate) (pDMAEA) include tertiary amine moieties, conferring positive charges to the polymer surface, thereby facilitating electrostatic interactions with cell surfaces[38]. The noncytotoxic epoxy functionality in poly(glycidyl methacrylate) (pGMA) readily captures amine groups via a ring-opening reaction and is thus capable of immobilizing bioactive molecules in culture medium to provide favorable surfaces for cell culture[39–42]. The copolymerization of pGMA with amine functional polymers results in enhanced formation of quaternary ammonium groups via the amine–epoxy reaction, further stabilizing the culture surface[31,43,44]. Poly(ethylene glycol dimethacrylate) (pEGDMA) is a crosslinked polymer with biocompatible ethylene glycol functionality[45,46]. When copolymers are formed, the EGDMA crosslinker moiety enhances the chemical and mechanical stability[47]. Halide-containing poly(4-vinylbenzyl chloride) (pVBC), which undergoes ionic crosslinking through the Menshutkin reaction when copolymerized with amine-containing monomers that enhance electrostatic interactions, was also adapted[34,48–50]. Poly(cyclohexyl methacrylate) (pCHMA), poly(benzyl methacrylate) (pBMA), and poly(2,4,6,8-tetravinyl-2,4,6,8-tetramethylcyclotetrasiloxane) (pV4D4) are characterized by their hydrophobic properties[35,51,52], offering unique hydrophobic protein-surface interactions[32,38,53]. Some polymer surfaces are exposed to plasma surface treatment, increasing surface energy and cell adhesion, thereby providing surfaces with hydrophilic properties[54,55].

ISCs$^{3D\text{-}hIO}$ differentiated from hiPSCs were seeded onto these predesigned biocompatible polymers possessing diverse functional properties to evaluate their suitability for xenogeneic-free ISC culture (Fig. 1c and Supplementary Fig. 2). For comparative analysis, we evaluated the colony sizes and the growth rate of ISCs$^{3D\text{-}hIO}$ cultured on each polymer substrate on Days 2 and 4. Additionally, we obtained the surface energy values of the polymer surfaces with contact angles of water and glycerol, which is a simple but important surface property that influences cell–surface interactions[29,32,35,56,57]. The surface energy values, colony areas, and growth rates were normalized on the basis of the maximum and minimum values for each variable and are depicted in a heatmap (Fig. 1d). The surface energy values of the polymer ranged between the minimum value of 27.7 mJ/m^2 for pCHMA and the maximum value of 97.1 mJ/m^2 for pDMAEMA. The three surfaces that demonstrated the largest colony areas on Day 2 were pEGDMA+p, Matrigel-coated

https://doi.org/10.1038/s41467-024-54653-9

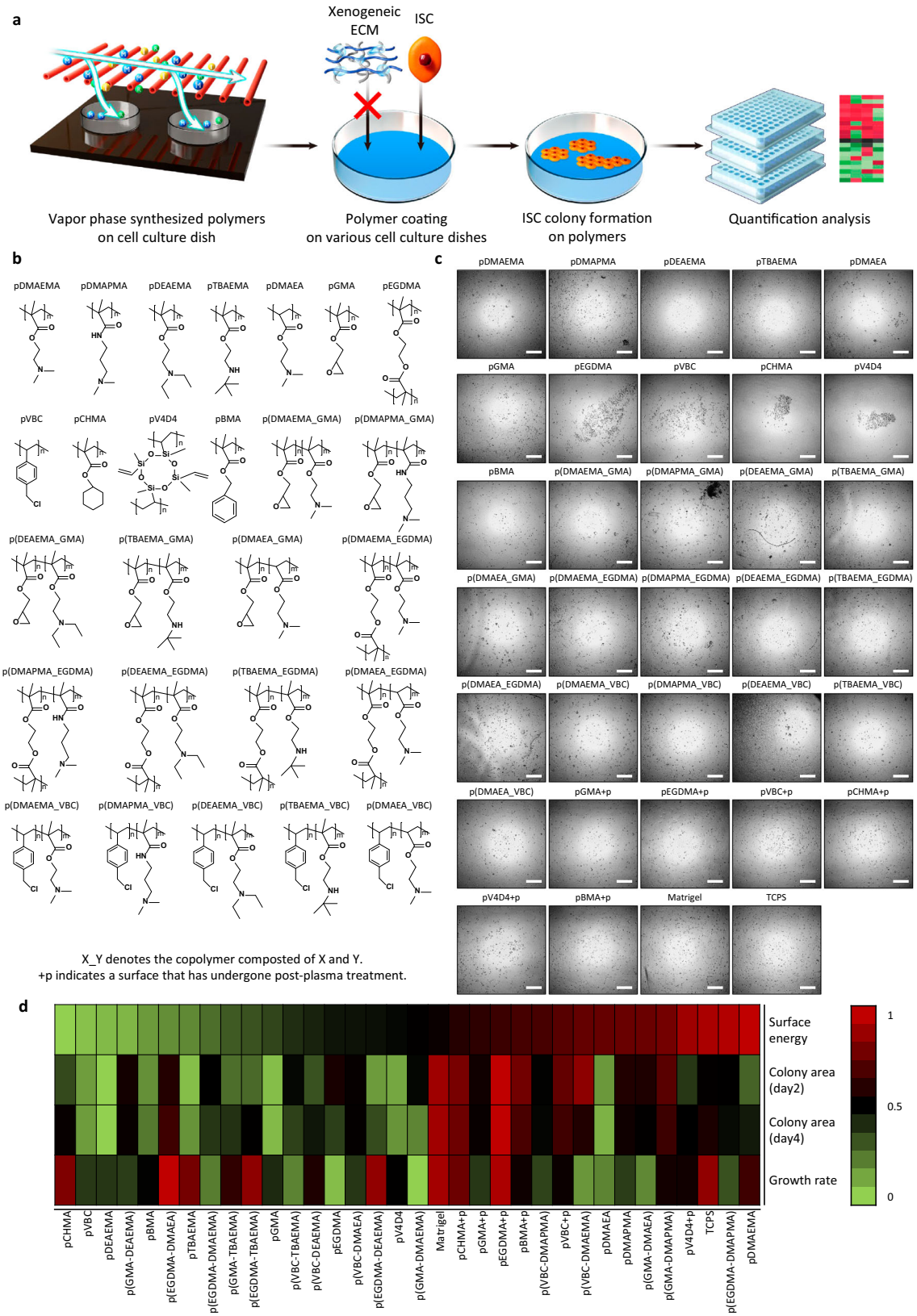

Fig. 1 | Polymer Screening for Xenogeneic-free Culture of ISCs$^{3D\text{-}hIO}$. a Schematic illustration of polymer synthesis in the vapor phase using the iCVD process and ISCs$^{3D\text{-}hIO}$ cultivation without xenogeneic ECM on polymers. **b** Chemical structures of 26 types of polymer candidates for the culture of ISCs$^{3D\text{-}hIO}$. (X_Y denotes the copolymer composed of X and Y, and +p indicates a surface that has undergone postplasma treatment.) **c** Morphologies of ISCs$^{3D\text{-}hIO}$ cultured on a Matrigel-coated surface, various polymer-coated surfaces and tissue culture polystyrene (TCPS) ($n = 2$ sample/group). Optical microscope images of each culture surface were captured on Day 4. The scale bar indicates 500 μm. **d** Heatmap of polymers with surface energy, colony areas at Days 2 and 4, and growth rates.

surface, and p(DMAEMA_VBC), with colony areas of 286,000 μm², 250,000 μm², and 230,000 μm², respectively. On Day 4, pEGDMA +p, Matrigel-coated surface, and pCHMA+p groups presented the largest colony areas of 641,000 μm², 552,000 μm² and 403,000 μm², respectively. The growth rates were calculated on the basis of colony areas on Days 2 and 4, revealing that p(DMAEA_EGDMA) presented the highest growth rate at 134%, followed by pEGDMA+p at 124% and the Matrigel-coated surface at 120%. Through comprehensive analysis of the heatmap results, pEGDMA+p surface exhibited high initial ISC adhesion, leading to a large colony area and a high growth rate, supporting ISC proliferation. Consequently, we designated this surface XF-DISC, considering it the most suitable for ISC$^{3D\text{-}hIO}$ culture. Our subsequent research efforts focused on exploring the XF-DISC surface for further investigation to ensure that XF-DISC can provide a Matrigel-free, stable surface for the long-term culture of ISCs$^{3D\text{-}hIO}$.

Evaluation of XF-DISC as a robust culture platform for ISCs$^{3D\text{-}hIO}$

To assess the potential of XF-DISC as a culture platform for ISCs$^{3D\text{-}hIO}$, we conducted a rigorous analysis with tissue culture polystyrene plates (TCPS) and Matrigel-coated TCPS as negative and positive control culture surfaces, respectively. XF-DISC exhibited no discernable differences in appearance compared with TCPS even after the iCVD process (Fig. 2a). However, a clear difference in wettability was observed, with the XF-DISC surface being more hydrophilic than the TCPS surface. This phenomenon was evidenced by the presence of red ink droplets, highlighting the advantageous characteristics of vapor–phase conformal coverage at room temperature (Fig. 2b). ISC$^{3D\text{-}hIO}$ colonies grew rapidly on both the Matrigel-coated surface and XF-DISC, whereas impeded growth was identified on the TCPS (Fig. 2c). ISCs$^{3D\text{-}hIO}$ demonstrated stable attachment and mobility after cell seeding, and colonies exhibited good adherence and dynamic movement on XF-DISC (Supplementary Movies 1–6). On Day 6, direct cell counting revealed 38,600 ± 2,800 cells on the Matrigel-coated surface, 37,000 ± 3,000 cells on XF-DISC, and 27,600 ± 3,000 cells on TCPS (Fig. 2d). Using the water-soluble tetrazolium-1 (WST-1) proliferation assay, a significant decrease in performance was observed on TCPS, whereas Matrigel-coated surfaces and XF-DISC exhibited increased proliferation rates (Fig. 2e). The quantitative analysis results were fully consistent with the observations of colony morphology. In addition to TCPS, we cultured ISCs$^{3D\text{-}hIO}$ on glass surfaces. Exceptional increases in colony areas were evident on the Matrigel- and XF-DISC-coated glass surfaces compared with the bare glass surface (Supplementary Fig. 3a). The colony areas quantified using crystal violet (CV) staining were 1.39 ± 0.23 cm² and 1.50 ± 0.05 cm² on the Matrigel-coated and XF-DISC surfaces, respectively (Supplementary Fig. 3b, c). In contrast, the bare glass surface had an area of only 0.51 ± 0.21 cm², which was less than half of the colony area observed on XF-DISC. These results confirmed that XF-DISC promotes the attachment and growth of ISCs$^{3D\text{-}hIO}$ independent of the substrate material. This finding strongly indicates the possibility of achieving consistent effects when these methods are applied to various cell culture substrates.

The XF-DISC surface was smooth, with a root mean square (RMS) roughness (R_q) less than 1 nm, as confirmed by atomic force microscopy (AFM) (Fig. 2f). The results of the quantitative analysis of colony areas derived from CV staining verified the excellent reproducibility of the XF-DISC culture system (Fig. 2g, h). In addition, XF-DISC showed exceptional long-term stability. Even after a storage period exceeding 2 years in ambient temperature air, XF-DISC demonstrated no apparent changes in its chemical composition and morphology or proliferation of ISCs$^{3D\text{-}hIO}$ (Fig. 2i, j and Supplementary Fig. 4), which is highly desirable for reliable long-term use and storage of XF-DISC. The reproducibility and long-term stability characteristics of XF-DISC emphasize the potential for broader utilization of xenogeneic-free surfaces. Upon culture on the XF-DISC surface, ISCs$^{3D\text{-}hIO}$ demonstrated a cell viability exceeding 99%, indicating that XF-DISC is suitable for cell proliferation (Fig. 2k, l). In the immunogenicity test using peripheral blood mononuclear cells (PBMCs)[58], the percentages of proliferating CD3-positive T cells were 1.86% and 1.93% in XF-DISC and TCPS, respectively, which were far lower than those in the phytohemagglutinin-L-stimulated group (5.73%) (Supplementary Fig. 5a). The inflammatory cytokine, tumor necrosis factor-α (TNF-α) secretion test was also performed to assess the immunogenicity of XF-DISC (Supplementary Fig. 5b, c). The levels of TNF-α secreted from RAW 264.7 mouse macrophages and THP-1 human monocytes after exposure to XF-DISC for 12 h and 48 h, respectively, were remarkably low and comparable to the level observed from cells on TCPS[59,60]. To validate the clinical application potential, we conducted an endotoxin level test on XF-DISC (Supplementary Fig. 5d). Considering that the acceptable endotoxin level for implantable medical devices is 0.5 EU/mL according to the Food and Drug Administration (FDA) guidelines, both XF-DISC and TCPS are acceptable for implantable devices with endotoxin levels less than 0.12 EU/mL[61].

Taken together, the results suggest that XF-DISC fully supported the culture of ISCs$^{3D\text{-}hIO}$ at levels comparable to those of the Matrigel coating. Furthermore, a substantial amount of cell production would be possible with the advantageous characteristics of XF-DISC, such as minimal batch variation, high long-term stability, biocompatibility, and the absence of biological safety concerns.

Xenogeneic-free culture system for scalability, long-term expansion, and stock banking of ISCs$^{3D\text{-}hIO}$

To determine the feasibility of the xenogeneic-free ISC$^{3D\text{-}hIO}$ culture system, we investigated the scalability, long-term expansion, and applicability of the stock banking system with $^{ISC3D\text{-}hIO}$ cultured on XF-DISC (Fig. 3a). Theoretical growth was extrapolated over a 30-day culture period using the increased cell count number observed in the first passage to assess the scalability of XF-DISC (Figs. 2d, 3b). The results indicated that the expected number of cells was 24-fold greater on both the XF-DISC surface and the Matrigel-coated surface. However, on the TCPS surface, only a 5-fold increase was observed. We then plotted experimental growth curves determined directly by counting the cell numbers during four consecutive passages and compared them with the theoretical growth curves obtained (Fig. 3c, d). Notably, a strong alignment between the experimental growth curve and the theoretical growth curve was observed. In addition, our consecutive passaging of ISCs$^{3D\text{-}hIO}$ on XF-DISC yielded an impressive average expansion efficiency of greater than 93% over four passages compared with that of Matrigel-coated surfaces. Regarding the regenerative transplantation method, the ability to obtain a consistent, reliable supply of ISCs, especially a large number of ISCs, that are suitable for transplantation without xenogeneic issues is of utmost importance. In this study, ISCs$^{3D\text{-}hIO}$ cultured on XF-DISC exhibited a high expansion rate, resulting in a 24-fold increase in cell number within 30 days, suggesting that XF-DISC is not only appropriate for the culture of ISCs$^{3D\text{-}hIO}$ but also holds great promise as a stem cell culture platform for the large-scale production of ISCs$^{3D\text{-}hIO}$ for extended cell therapeutics. Moreover, XF-DISC was capable of supporting long-term expansion, retaining the continuous formation of ISC$^{3D\text{-}hIO}$ colonies for at least 30 consecutive passages without any morphological abnormalities (Fig. 3e). The demonstration of 30 successive passages every 7 to 10 days provided robust evidence that ISC$^{3D\text{-}hIO}$ can be sustained for a minimum of 210 days, underscoring the remarkable stability and reliability of XF-DISC.

Next, we subjected the cell stocks to freezing and thawing to validate the feasibility of the stock banking system. Upon thawing the cell stock, we verified the formation of ISC$^{3D\text{-}hIO}$ colonies on both the Matrigel-coated surface and XF-DISC (Fig. 3f). Quantification of the number of attached cells revealed efficiencies of greater than 82% on both the Matrigel-coated surface and the XF-DISC (Fig. 3g). In the proliferation assay, normalization to the values of the Matrigel-coated

https://doi.org/10.1038/s41467-024-54653-9

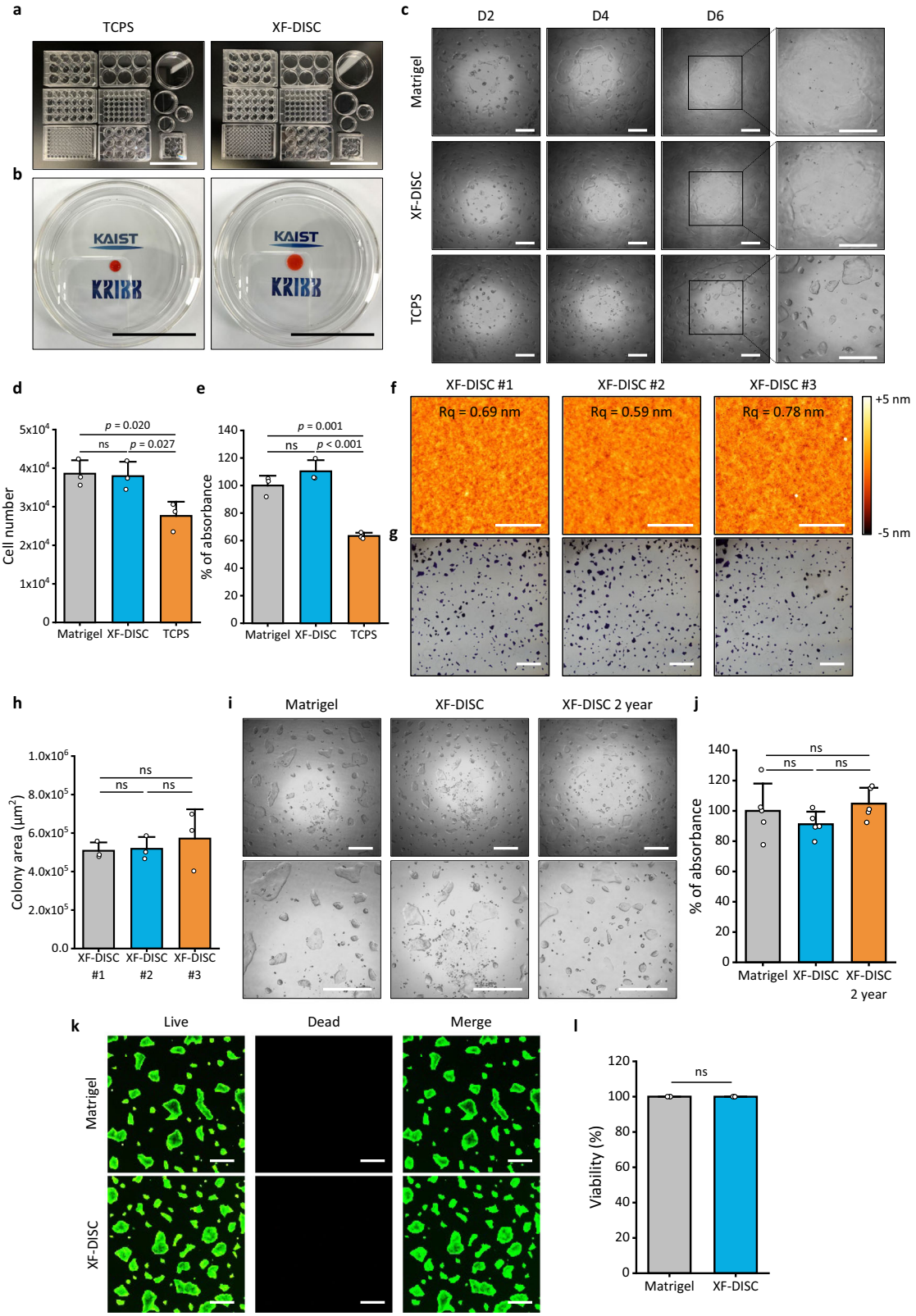

surface did not significantly differ from those of XF-DISC (Fig. 3h). Subsequently, ISCs$^{3D\text{-}hIO}$ demonstrated normal colony formation in successive passages (Supplementary Fig. 6a). CV staining also revealed that more than 80% of both the Matrigel-coated surface and the XF-DISC covered the surface (Supplementary Fig. 6b, c). In addition, upon thawing stocks that had been stored for more than 3 years, the efficiency values were greater than 35%, and there was no significant difference between the Matrigel-coated surface and XF-DISC in supporting ISC$^{3D\text{-}hIO}$ proliferation, illustrating long-term cell stock stability (Fig. 3i, j).

The culture of iPSC-derived ISCs$^{3D\text{-}hIO}$ in a xenogeneic-free environment is of prime importance given the advantages of the potential

Fig. 2 | Evaluation of the Versatility, Viability, and Safety in ISCs$^{3D\text{-}hIO}$ Cultured on XF-DISC. a External appearance of TCPS (left) and XF-DISC (right). Scale bar: 10 cm. **b** Wettability differences between TCPS and XF-DISC were observed by dropping 30 μL of red ink dissolved in water on each surface. Scale bar: 5 cm. **c** Morphologies of ISCs$^{3D\text{-}hIO}$ cultured on a Matrigel-coated surface (top), XF-DISC (middle), and TCPS (bottom) at Days 2, 4, and 6. The images in the right column are the zoomed-in images taken on Day 6. Scale bar: 500 μm. **d** Quantification of ISC$^{3D\text{-}hIO}$ cell numbers on Day 6 after the seeding of cells on the Matrigel-coated surface, XF-DISC and TCPS. Data represent the mean ± SD ($n = 3$ biological samples), and a two-tailed t-test was applied to measure p values. **e** WST-1 assay of ISCs$^{3D\text{-}hIO}$ cells cultured for 7 days on the Matrigel-coated surface, XF-DISC and bare TCPS. Data represent the mean ± SD ($n = 3$ biological samples), and a two-tailed t-test was applied to measure p values. **f** AFM images of XF-DISC surfaces from 3 different batches. Scale bar: 1 μm. **g** Crystal violet staining images of ISCs$^{3D\text{-}hIO}$ cultured on XF-DISC from 3 different batches. Scale bar: 500 μm. **h** Quantification of colony areas on XF-DISC from 3 different batches. Data represent the mean ± SD ($n = 3$ biological samples), and a two-tailed t-test was applied to measure p values. **i** Morphologies of ISCs$^{3D\text{-}hIO}$ cultured for 7 days on a Matrigel-coated surface (left), XF-DISC (middle) and XF-DISC stored for 2 years (right), passage 1. Scale bar: 500 μm. **j**, WST-1 assay of ISCs$^{3D\text{-}hIO}$ cultured for 7 days on a Matrigel-coated surface, XF-DISC and XF-DISC stored for 2 years. Data represent the mean ± SD ($n = 5$ biological samples), and a two-tailed t-test was applied to measure p values. **k** Fluorescence microscopy images of ISCs$^{3D\text{-}hIO}$ cultured on Matrigel-coated surfaces and XF-DISC. ISC$^{3D\text{-}hIO}$ viability was assessed on Day 6 after seeding. Scale bar: 500 μm. **l** Quantification of the viability of ISCs$^{3D\text{-}hIO}$ cultured on a Matrigel-coated surface and XF-DISC. Data represent the mean ± SD ($n = 3$ biological samples), and a two-tailed t-test was applied to measure p values.

use for universal regenerative therapies and the development of personalized therapies because hiPSCs can differentiate into all body cell types, enabling personalized medicine. Given that expanding the application scope of XF-DISC is also important, we present work in progress toward extending the application of XF-DISC to verify its adaptability across different stem cell types. First, greater than 99% H9-ISC$^{3D\text{-}hIO}$ viability was observed when cultured on XF-DISC (Supplementary Fig. 7a, b). Additionally, the exceptional potential of our platform was confirmed again, supporting 10 consecutive passages of H9-ISCs$^{3D\text{-}hIO}$ (Supplementary Fig. 7c). This observation strongly suggested broader expansibility of XF-DISC and its applicability to ISCs from diverse origins.

Together, these results clearly indicate that XF-DISC can effectively support xenogeneic-free culture of ISCs$^{3D\text{-}hIO}$ while allowing for high scalability and long-term expansion. Moreover, the scalable XF-DISC enabled the establishment of a prolonged stock-banking system for future clinical applications.

Cellular trait evaluation of ISCs$^{3D\text{-}hIO}$ on XF-DISC

To further elucidate the feasibility of XF-DISC as an ISCs$^{3D\text{-}hIO}$ culture platform, we conducted a thorough characterization of ISCs$^{3D\text{-}hIO}$ cultured on XF-DISC and Matrigel-coated surfaces. We investigated whether ISCs$^{3D\text{-}hIO}$ cultured on XF-DISC exhibited messenger ribonucleic acid (mRNA) expression related to intestinal epithelial markers with a lack of the expression of markers associated with human pluripotent stem cell (hPSC) stemness. We conducted quantitative polymerase chain reaction (qPCR) analysis of the ISCs$^{3D\text{-}hIO}$ cultured on Days 4, 6, and 8 and visualized the results through a heatmap (Fig. 4a). Upon examination of the heatmap of mRNA expression, it was apparent that markers associated with intestinal epithelial features, such as *LGR5, EPHB3, SOX9, CD24, CD44, CD133*, and *CD166*, were expressed at higher levels in ISCs$^{3D\text{-}hIO}$ than in hPSCs. In contrast, the expression of the stemness markers for hPSCs, *OCT4*, and *NANOG*, and the proliferation marker *MKI67* was much lower in ISCs$^{3D\text{-}hIO}$ than in hPSCs, confirming the successful establishment of ISCs$^{3D\text{-}hIO}$ from hPSCs. During long-term culture, to verify whether ISCs$^{3D\text{-}hIO}$ maintains epithelial features, a comparison of marker expression between cells cultured on XF-DISC and those cultured on Matrigel-coated surfaces was conducted (Fig. 4b). Following passaging, the expression levels of ISC markers (*LGR5*, *EPHB3*, *CD44* and *SOX9*) and the proliferation marker *MKI67* remained comparable between ISCs$^{3D\text{-}hIO}$ cultured on the two surfaces. In addition, maintenance of epithelial features was also observed in H9-ISCs$^{3D\text{-}hIO}$ (Supplementary Fig. 7d). These results indicated that XF-DISC supports mass culture of ISCs$^{3D\text{-}hIO}$ through successive passages while preserving the unique ISC characteristics.

Fluorescence-activated cell sorting (FACS) analysis confirmed the presence of stem cells expressing CD44 and SOX9 within the ISC$^{3D\text{-}hIO}$ population, whereas cells expressing the endothelial marker CD34 were notably scarce (Fig. 4c). In more detail, FACS analysis revealed that 91.4% and 93.6% of the cells from ISCs$^{3D\text{-}hIO}$ cultured on the Matrigel-coated surface and XF-DISC, respectively, were CD44 positive. Regarding the SOX9-positive cell population, the results revealed that 97.0% of cells on the Matrigel-coated surfaces and 95.0% of cells on XF-DISC were positive for SOX9 expression, demonstrating that over 90% of the cells were in a stemness-enriched state. Furthermore, ISC$^{3D\text{-}hIO}$ colonies stained positive for the cell proliferation marker Ki67 and exhibited an appropriate expression pattern of the intestinal stem cell marker SOX9. The expression patterns of the fetal stem cell markers EIF3E and LDHB were also similar on the two surfaces (Fig. 4d). FABP1, a marker of enterocytes, was also expressed in ISC colonies, whereas specific markers of goblet cells (MUC2) and enteroendocrine cells (CHGA) were not detected in ISC$^{3D\text{-}hIO}$ colonies. Importantly, the staining patterns were similar when comparing ISCs$^{3D\text{-}hIO}$ cultured on XF-DISC with those cultured on the Matrigel-coated surface.

To analyze ISC$^{3D\text{-}hIO}$ characteristics at a comprehensive level, we performed RNA sequencing (RNA-seq) and proteomics analyses using ISCs$^{3D\text{-}hIO}$ cultured on XF-DISC and Matrigel-coated culture dishes. A volcano plot of the RNA-seq data revealed no significant differences in global gene expression patterns between ISCs$^{3D\text{-}hIO}$ cultured on XF-DISC and those cultured on Matrigel-coated surfaces (Fig. 4e). The results of multidimensional scaling (MDS) using our original and publicly available RNA-seq datasets of hiPSCs, hESCs, air–liquid interface (ALI)-differentiated intestinal tissue and human small intestine (hSI) samples demonstrated that ISCs$^{3D\text{-}hIO}$ cultured on XF-DISC were most closely related to ISCs$^{3D\text{-}hIO}$ cultured on Matrigel-coated surface, whereas ISCs$^{3D\text{-}hIO}$ exhibited distinct patterns compared with the hPSC, ALI or hSI samples (Fig. 4f). In addition, at the protein level, no significant differences were observed between ISCs$^{3D\text{-}hIO}$ cultured on XF-DISC and those cultured on the Matrigel-coated surface (Fig. 4g).

Taken together, these data showed that the gene and protein expression of ISCs$^{3D\text{-}hIO}$ and the cellular patterns within colonies exhibited negligible differences between those cultured on the Matrigel and XF-DISC surfaces, and these characteristics remained consistent even following consecutive passaging.

Xenogeneic-free formation of functional intestinal tissue on XF-DISCs through ALI differentiation

We investigated the ability of XF-DISC to support the formation of intestinal tissue through the ALI differentiation method[17]. XF-DISC-coated inserts were used to culture ISCs$^{3D\text{-}hIO}$ in the absence of xenogeneic ECM, and the ALI differentiation process was induced to promote the formation of intestinal tissue-like structures (Fig. 5a). Owing to the advantageous characteristic of the iCVD process, which enables fully conformal coating in a solvent-free manner without any apparent damage, the XF-DISC-coated inserts revealed no observable differences from the bare inserts (Fig. 5b). Following 8 days of ALI differentiation, the intestinal epithelium derived from ISCs$^{3D\text{-}hIO}$ cultured on XF-DISC-coated inserts exhibited a characteristic serpentine morphology resembling native intestinal structures (Fig. 5c). We

https://doi.org/10.1038/s41467-024-54653-9

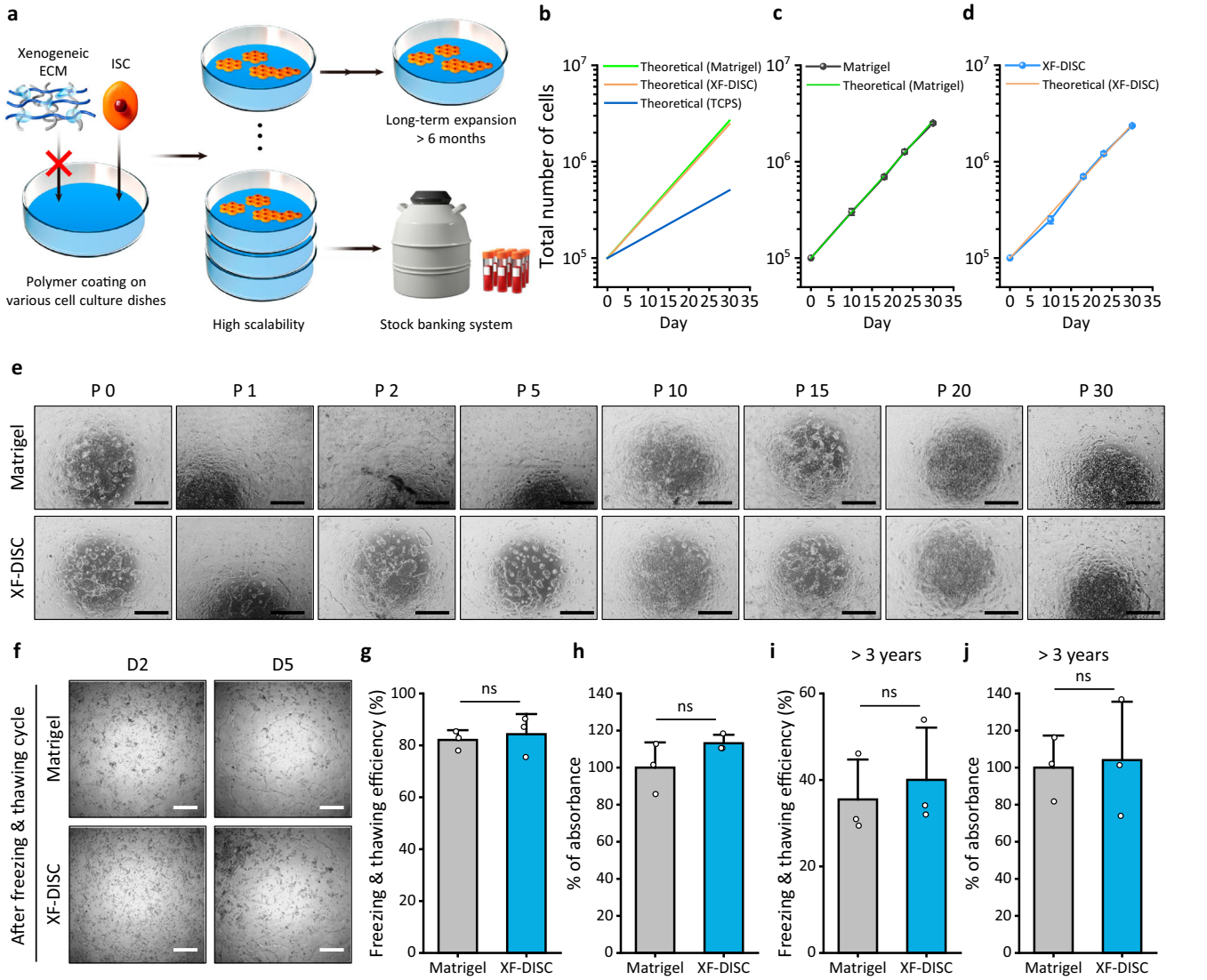

Fig. 3 | Assessment of long-term expansion and stock banking potential for ISCs$^{3D\text{-}hIO}$ cultured on XF-DISC. a Schematic illustration of the long-term expansion capability and implementation of a stock banking system for ISCs$^{3D\text{-}hIO}$ cultured on XF-DISC. **b** Theoretical growth curve of ISCs$^{3D\text{-}hIO}$ cultured on a Matrigel-coated surface; XF-DISC and TCPS were estimated, and the cell numbers were quantified. **c d** Theoretical growth rate and experimentally determined growth rate after ISCs$^{3D\text{-}hIO}$ were passaged for four passages on a Matrigel-coated surface and XF-DISC, respectively. **e** Morphologies of ISCs$^{3D\text{-}hIO}$ on a Matrigel-coated surface and XF-DISC over the course of long-term expansion culture across 30 sequential passages. Scale bar: 1 mm ($n = 3$ samples/group). **f** Morphologies of ISCs$^{3D\text{-}hIO}$ on a Matrigel-coated surface and XF-DISC after freezing and thawing cycles on Days 2 and 5 ($n = 3$ samples/group). Before freezing, the number of passages was 10. Scale bar: 500 μm. **g** Quantitative efficiency of viable cells after freezing and thawing. Data represent the mean ± SD ($n = 3$ biological samples), and a two-tailed t-test was applied to measure p values. **h** WST-1 assay of thawed ISCs$^{3D\text{-}hIO}$ cultured for 5 days on a Matrigel-coated surface and XF-DISC. Data represent the mean ± SD ($n = 3$ biological samples), and a two-tailed t-test was applied to measure p values. **i** Quantitative efficiency of viable cells after the freezing and thawing of stocks stored for more than 3 years. Data represent the mean ± SD ($n = 3$ biological samples), and a two-tailed t-test was applied to measure p values. **j** WST-1 assay of thawed ISCs$^{3D\text{-}hIO}$ cultured for 5 days on a Matrigel-coated surface and XF-DISC. Stocks were stored for more than 3 years. Data represent the mean ± SD ($n = 3$ biological samples), and a two-tailed t-test was applied to measure p values.

performed qPCR analysis on ALI-differentiated intestinal tissues and compared them with human small intestine tissues. The expression profiles of markers associated with ISCs (*LGR5, CD44, SOX9, AXIN2*, and *CTNNB*), proliferation (*MKI67*), differentiation (*VIL1, FABP1, KRT20, LYZ*, and *MUC2*), intestinal maturation (*OLFM4*), and epithelial cells (*CDH1*) were examined in the intestinal epithelium formed on both the XF-DISC and Matrigel-coated surfaces (Fig. 5d). The presence of gene expression related to stem cells, proliferation, and differentiated cells clearly confirmed the successful development of functional intestinal tissues.

To further assess the expression patterns of differentiated intestinal tissues, we stained cryosectioned samples of the intestinal epithelium on Days 0, 4, and 8 (Fig. 5e). Over time, the increased structure became more prominent and intricate with increased expression of differentiation markers (KRT20 and VIL1). Based on the expression of a stem cell marker (CD44) and a proliferation marker (Ki67), we confirmed the ability to maintain homeostasis within a xenogeneic-free environment, underscoring the similarity to the native intestinal structure. The hematoxylin and eosin (H&E) staining results clearly revealed a similar trend of increasing height and complexity of the tissue structure (Fig. 5f). Even with the use of a different cell line, namely, H9-ISCs$^{3D\text{-}hIO}$, for ALI differentiation, we confirmed a distinctively differentiated morphology, illustrating the adaptability of XF-DISC for generating intestinal tissue across diverse cell sources (Supplementary Fig. 8a). No significant differences in the gene expression or expression patterns of differentiated H9-ISC$^{3D\text{-}hIO}$ were

https://doi.org/10.1038/s41467-024-54653-9

observed between the XF-DISC surface and the Matrigel-coated surface (Supplementary Fig. 8b, c). The TEER values, a representative indicator of epithelial integrity[62], were 295 ± 25 ohm × cm² for the Matrigel-coated surface and 293 ± 4 ohm × cm² for XF-DISC on Day 8 (Fig. 5g). During the ALI differentiation process, the TEER values remained constant for the two surfaces, indicating superior epithelial integrity and well-formed functional characteristics of the intestinal tissues.

Together, these results suggest that XF-DISC can fully support the formation of the intestinal epithelium, facilitating its application in various in vitro intestinal models without the need for xenogeneic ECM.

Therapeutic effect of xenogeneic-free cultured ISCs$^{3D\text{-}hIO}$

We transplanted ISCs$^{3D\text{-}hIO}$ grown on XF-DISC for 4–6 days into the ethylenediamine tetraacetic acid (EDTA)-injured colonic epithelium of immunodeficient (NIG) mice and examined the progress of injury recovery via colonoscopy at Days 0 and 14 posttransplantation (PT) (Fig. 6a). On Day 0, EDTA-induced injuries exhibited the same degree of epithelial damage in both the fibrin-only and ISC$^{3D\text{-}hIO}$ on XF-DISC

Fig. 4 | Comprehensive Characterization of ISCs$^{3D\text{-}hIO}$ Cultured on XF-DISC. **a** Heatmap of gene expression in hPSCs and ISCs$^{3D\text{-}hIO}$ cultured on Matrigel-coated surfaces and XF-DISC for 4, 6, and 8 days at passage 3, as quantified by qRT–PCR ($n = 3$). **b** Gene expression of intestinal markers (*LGR5, EPHB3, CD44* and *SOX9*) and a proliferation marker (*MKI67*) of ISCs$^{3D\text{-}hIO}$ cultured on a Matrigel-coated surface and XF-DISC for 7 days at passages 3, 8 and 18 quantified by qRT–PCR. Data represent the mean ± SD ($n = 3$ biological samples), and a two-tailed *t*-test was applied to measure *p* values. **c** Cell population of markers (CD44, SOX9 and CD34) of ISCs$^{3D\text{-}hIO}$ cultured on a Matrigel-coated surface and XF-DISC for 7 days, as determined by FACS analysis (Red: negative control cells in each sample, black: specific antibody stained-ISCs$^{3D\text{-}hIO}$ cultured on Matrigel-coated surface and blue: specific antibody stained-ISCs$^{3D\text{-}hIO}$ cultured on XF-DISC). **d** Representative images showing the immunostaining of SOX9, Ki67, EIF3E, FABP1, LDHB, CHGA and MUC2 expression in ISCs cultured on a Matrigel-coated surface and XF-DISC for 7 days at passage 2 ($n = 3$ samples/group). Scale bar: 100 μm. **e** Volcano plot depicting gene abundance changes in ISCs cultured on a Matrigel-coated surface and XF-DISC for 7 days at passage 17. The vertical red lines indicate ± 4-fold changes, and the horizontal red line indicates a minimum significance of 20 (p value = 0.01). Multidimensional scaling analysis of the pairwise distances of the sample was conducted. **f** MDS plot of the pairwise distances between samples. Six homogeneous sample groups were observed; Matrigel (black, $n = 3$), XF-DISC (red, $n = 3$), ALI (blue, $n = 3$), hSI (green, $n = 2$), iPSC (CRL, pink, $n = 1$), and ESC (H9, yellow, $n = 1$). **g** Volcano plot depicting protein abundance changes in ISCs cultured on a Matrigel-coated surface and XF-DISC for 3 days at passage 12. The vertical red lines indicate ± 4-fold changes, and the horizontal red line indicates a minimum significance of 20 (p value = 0.01). Label-free quantification-based proteomic analysis was performed via ANOVA.

groups (3 mice in each group). After orthotopic transplantation of ISCs$^{3D\text{-}hIO}$, enhanced thickening of the colon and no colonic bleeding were observed on Day 14 (Fig. 6b). Histological analysis with H&E and alcian blue/periodic acid-Schiff (AB-PAS) staining demonstrated that ISCs$^{3D\text{-}hIO}$ successfully engrafted and induced regeneration of the rectal epithelium. The ISC$^{3D\text{-}hIO}$ xenografts shaped the whole crypt and secreted mucin, as shown in Fig. 6c. A previous study indicated that the xenografted human colon formed larger crypt structures than the mouse colon[12]. Notably, ISC$^{3D\text{-}hIO}$ on XF-DISC ($n = 246$ crypts from 3 mice) exhibited markedly greater crypt depth than the fibrin-only group ($n = 303$ crypts from 3 mice) (Fig. 6d). Immunofluorescence staining further verified that the cells expressing human-specific E-cadherin (hECAD)$^{+}$ were detected only in the ISCs$^{3D\text{-}hIO}$ in the XF-DISC group (Fig. 6e). Thus, these data confirm that ISCs$^{3D\text{-}hIO}$ on XF-DISC are potent cell sources for the treatment of intestinal injury. Additionally, visual observation confirmed normalcy in major adjacent organs (liver, kidney, spleen, stomach, and small intestine) (Fig. 6f).

Next, we established a DSS-induced colitis model in NIG mice and xenotransplanted ISCs$^{3D\text{-}hIO}$ into these mice (Fig. 7a). Although a large area of ulcers was noted on Day 0 and the severity was quite high in the ISC$^{3D\text{-}hIO}$ on XF-DISC group, symptoms were quickly alleviated on Day 14 PT, and ulceration was reduced considerably along with mucosal changes according to colonoscopic analysis (Fig. 7b, Supplementary Movies 7, 8). On Day 28 PT with ISCs$^{3D\text{-}hIO}$ grown on XF-DISC, the colonic epithelium was apparently thickened, with low vasculature and practically no ulceration. Histopathological analysis with H&E staining also revealed that xenografted ISCs$^{3D\text{-}hIO}$ regenerated the colonic epithelium, and functional goblet cells were detected via AB-PAS staining, as evidenced by mucin secretion (Fig. 7c). Notably, the crypt depth in the ISC$^{3D\text{-}hIO}$ on XF-DISC group ($n = 714$ crypts from 6 mice) was also far greater than that in the fibrin-only group ($n = 228$ crypts from 3 mice) (Fig. 7d). In the immunofluorescence analysis, positive detection of hECAD was exclusively observed in the ISC$^{3D\text{-}hIO}$ on the XF-DISC xenograft group (Fig. 7e).

Collectively, the in vivo data revealed that ISCs$^{3D\text{-}hIO}$ grown on XF-DISC were successfully implanted into EDTA-injured mice, and these cells were integrated with and restored the colon tissue in the DSS-induced colitis model, clearly confirming that the ISCs$^{3D\text{-}hIO}$ grown on XF-DISC represent promising therapeutics for intestinal diseases.

Discussion

The development of a reliable biocompatible culture system for ISCs is crucial for the clinical implementation of regenerative medicine, given the pivotal role of ISCs in maintaining and regenerating the intestinal epithelium. For ISC transplantation to serve as a novel regenerative treatment for humans, obstacles mainly posed by the utilization of xenogeneic materials must be overcome. In previous studies, synthetic hydrogels characterized by a defined chemical composition and reconstruction of the stem cell microenvironment were used to culture ISCs$^{3D\text{-}hIO}$ under xenogeneic-free defined conditions[21,22,26,63,64]. However, the limitations of 3D culture, including its temporal and operational inefficiencies, render synthetic hydrogel platforms less advantageous for large-scale production of cells intended for application in stem cell therapeutics.

In this study, we created a reliable cell culture surface, XF-DISC, using iCVD-based polymer screening, and the surface efficiently supports the rapid expansion and mass production of clinical-grade ISCs$^{3D\text{-}hIO}$. The expansion rate of these cells on the XF-DISC closely mirrored the theoretical growth curve obtained for consecutive passages. The XF-DISC platform demonstrated stable adhesion and proliferation, even upon thawing stocks preserved for more than 3 years. Most importantly, XF-DISCs could be cultured for an extended period of at least 30 passages without compromising their proliferative ability. The cells on XF-DISC were fully effective after freeze-thaw cycle and can be amplified rapidly for the steady mass production of high-performance ISCs. One of the limitations of hIO is quality control (QC), but the opportunity created by XF-DISC for the simple and easy production of ISCs$^{3D\text{-}hIO}$ offers reliable cell properties that enable effective QC. Moreover, during the process of verifying differentiation capability of ISCs$^{3D\text{-}hIO}$ cultured on XF-DISC to differentiate efficiently into 2.5D intestinal epithelium using the ALI method, indicating its potential for use *in* in vitro disease modeling.

Notably, we demonstrated that the ISCs$^{3D\text{-}hIO}$ on XF-DISC represent a promising candidate for advancing the field of regenerative medicine, particularly in the context of epithelial defects, such as inflammatory bowel disease. All the in vivo data demonstrated that ISCs$^{3D\text{-}hIO}$ on XF-DISC rapidly engrafted into the damaged intestine, demonstrating that this treatment is capable of regenerating affected areas and restoring functionality. The cells could survive within the in vivo environment, induce intestine-like tissue regeneration, and function in the host intestine in an inflammatory environment, strongly suggesting their beneficial effects as therapeutic agents for intestinal diseases. Of course, from a safety perspective, more studies on long-term monitoring are needed for clinical application. Nevertheless, the development of xenogeneic-free conditions for the culture and transplantation of human ISCs ultimately highlights the feasibility of regenerative medicine. Given that ISC$^{3D\text{-}hIO}$ can be derived from both hiPSCs and hESCs, ISC$^{3D\text{-}hIO}$ on XF-DISC could be a promising autologous and allogeneic cell source for ISC therapy. To the best of our knowledge, the XF-DISC platform stands out as the only system that employs xenogeneic-free materials without BME, simultaneously featuring a clearly defined chemical composition of the culture medium and enabling long-term culture and application of the stock banking system (Supplementary Tables 3–5). To the best of our knowledge, the XF-DISC is the most advanced stem cell culture platform for the massive production of human ISCs, making it an innovative standard. As an exceptional Matrigel-free platform, XF-DISC provides new avenues for the advancement of clinical-grade cell therapeutics and offers tremendous potential for the field of regenerative medicine, particularly in addressing intestinal diseases and related disorders.

https://doi.org/10.1038/s41467-024-54653-9

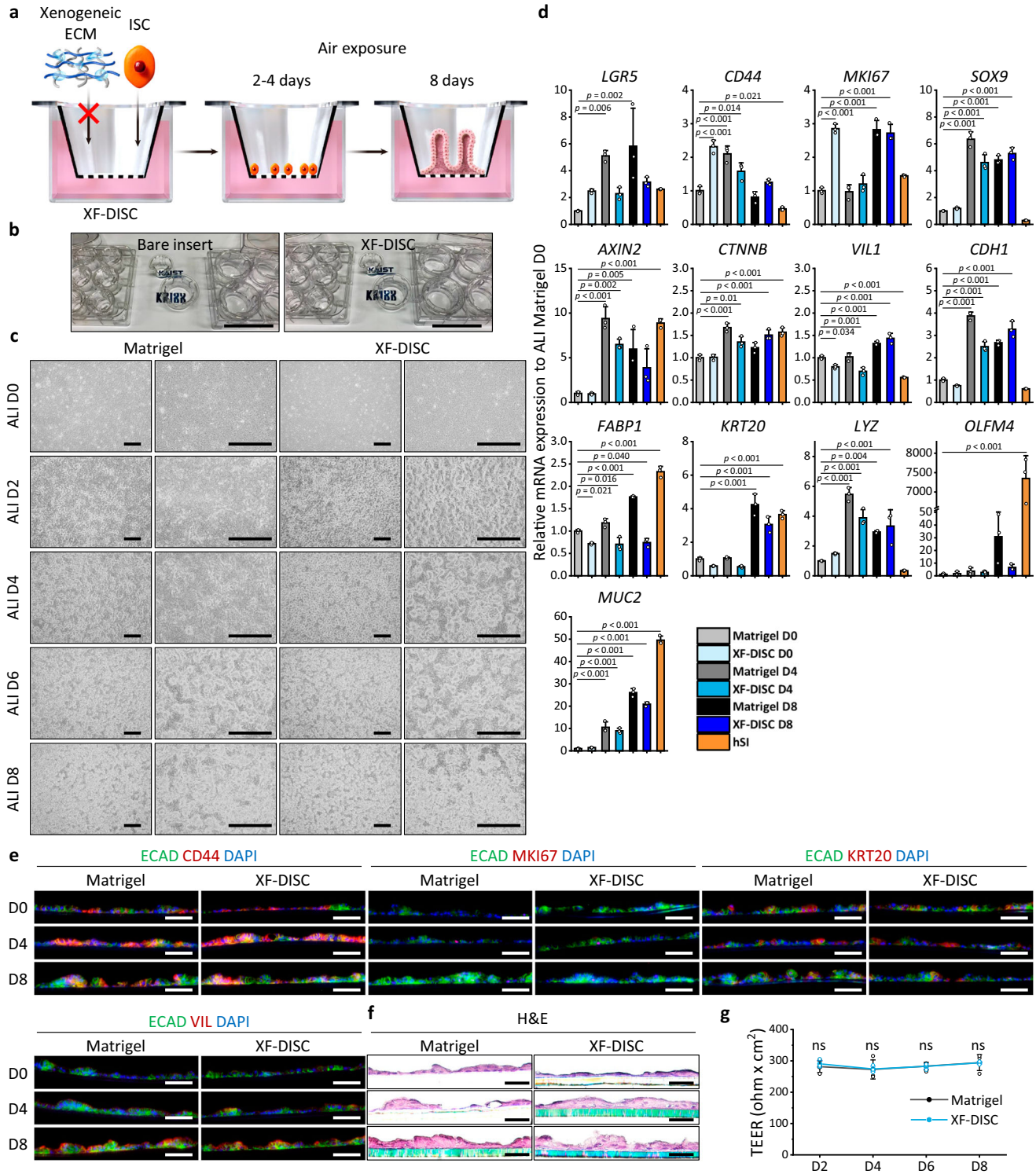

Fig. 5 | Formation of Intestinal Tissues on XF-DISC. a Workflow of intestinal tissue formation on XF-DISC. **b** External appearance of bare (left) and XF-DISC (right) inserts. Scale bar: 5 cm. **c** Surface views of 3D intestinal tissues subjected to ALI differentiation on a Matrigel-coated surface and XF-DISC for 0, 2, 4, 6, and 8 days at passage 17 ($n = 3$ samples/group). Scale bar: 500 μm. **d** Gene expression of markers of human small intestine and ALI differentiated intestinal tissues on a Matrigel-coated surface and XF-DISC for 0, 4 and 8 days at passage 6, as quantified by qRT–PCR. Data represent the mean ± SD ($n = 3$ biological samples). Statistical significance between Matrigel D0 cells and other cells was assessed by one-way ANOVA followed by Tukey's post hoc test. **e** Representative images showing immunostained sections of ALI differentiated intestinal tissues on a Matrigel-coated surface and XF-DISC for 0, 4 and 8 days at passage 6 ($n = 3$ samples/group). Scale bar: 100 μm. **f** Representative images showing histological sections of ALI differentiated intestinal tissues on a Matrigel-coated surface and XF-DISC for 0, 4 and 8 days at passage 6. Scale bar: 20 μm ($n = 3$ samples/group). **g** TEER values of ALI-differentiated intestinal tissues on a Matrigel-coated surface and XF-DISC for 2, 4, 6, and 8 days at passage 5. Data represent the mean ± SD ($n = 3$ biological samples), and a two-tailed *t*-test was applied to measure *p* values.

https://doi.org/10.1038/s41467-024-54653-9

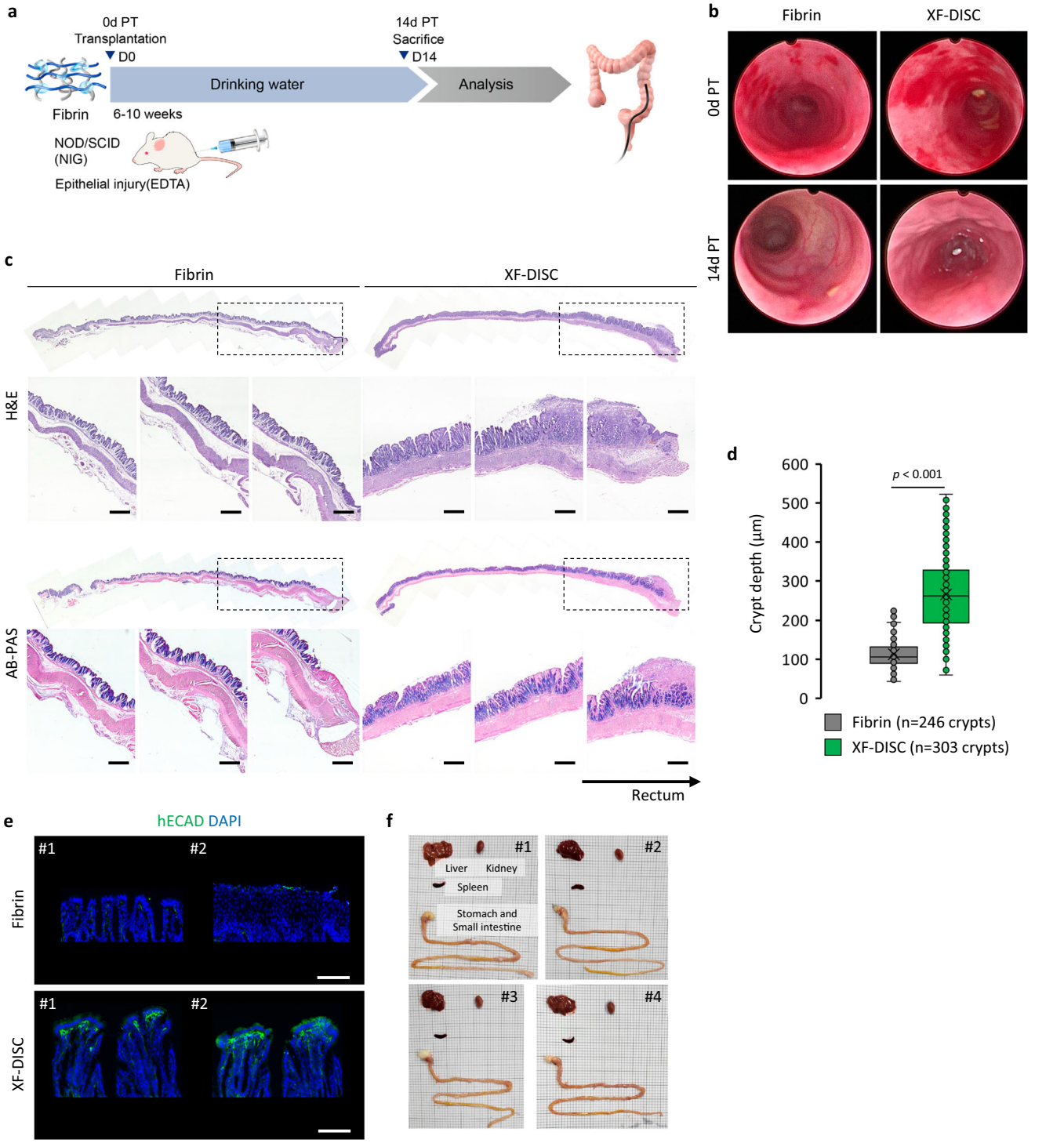

Fig. 6 | Transplantation of ISCs$^{3D\text{-}hIO}$ Cultured on XF-DISC in EDTA-induced Intestinal Epithelial Injury. a Workflow of ISC$^{3D\text{-}hIO}$ transplantation in NOD/SCID mice. **b** Representative mouse colonoscopic observations over time. **c** Top, histopathology of the xenograft colon tissues based on H&E staining ($n = 5$ samples/group). Bottom, mucin staining of the xenograft colon tissues based on AB–PAS staining ($n = 2$ samples/group). Scale bar: 500 μm. **d** Box and scatterplots of the crypt depth of fibrin-only (n = 246 crypts from three mice; 87, 80, and 79 crypts respectively) and ISCs$^{3D\text{-}hIO}$ on XF-DISC (n = 303 crypts from three mice; 89, 117, and 97 crypts respectively) treated xenograft colon tissues following H&E staining. The quartiles of the boxplot are mean ± SD, and a Welch's unpaired *t*-test was applied to measure *p* value. **e** Human E-cadherin staining of xenograft tissues, indicating xenotransplanted ISCs$^{3D\text{-}hIO}$ cultured on XF-DISC ($n = 2$ from each group). Scale bar: 100 μm. **f**, Bright-field images of the main organs after xenotransplantation ($n = 4$).

Nevertheless, XF-DISC faces potential challenges in translational applications that need to be addressed. For the application of cells derived from XF-DISC to human therapy, it is essential to conduct clinical trials involving not only mice but also larger animals. These trials are necessary to validate the cell scale required for therapeutic use and to assess the potential regenerative effects.

Moreover, we noted that small intestine characteristics appeared after in vitro differentiation of ISCs$^{3D\text{-}hIO}$ via the ALI culture system and

https://doi.org/10.1038/s41467-024-54653-9

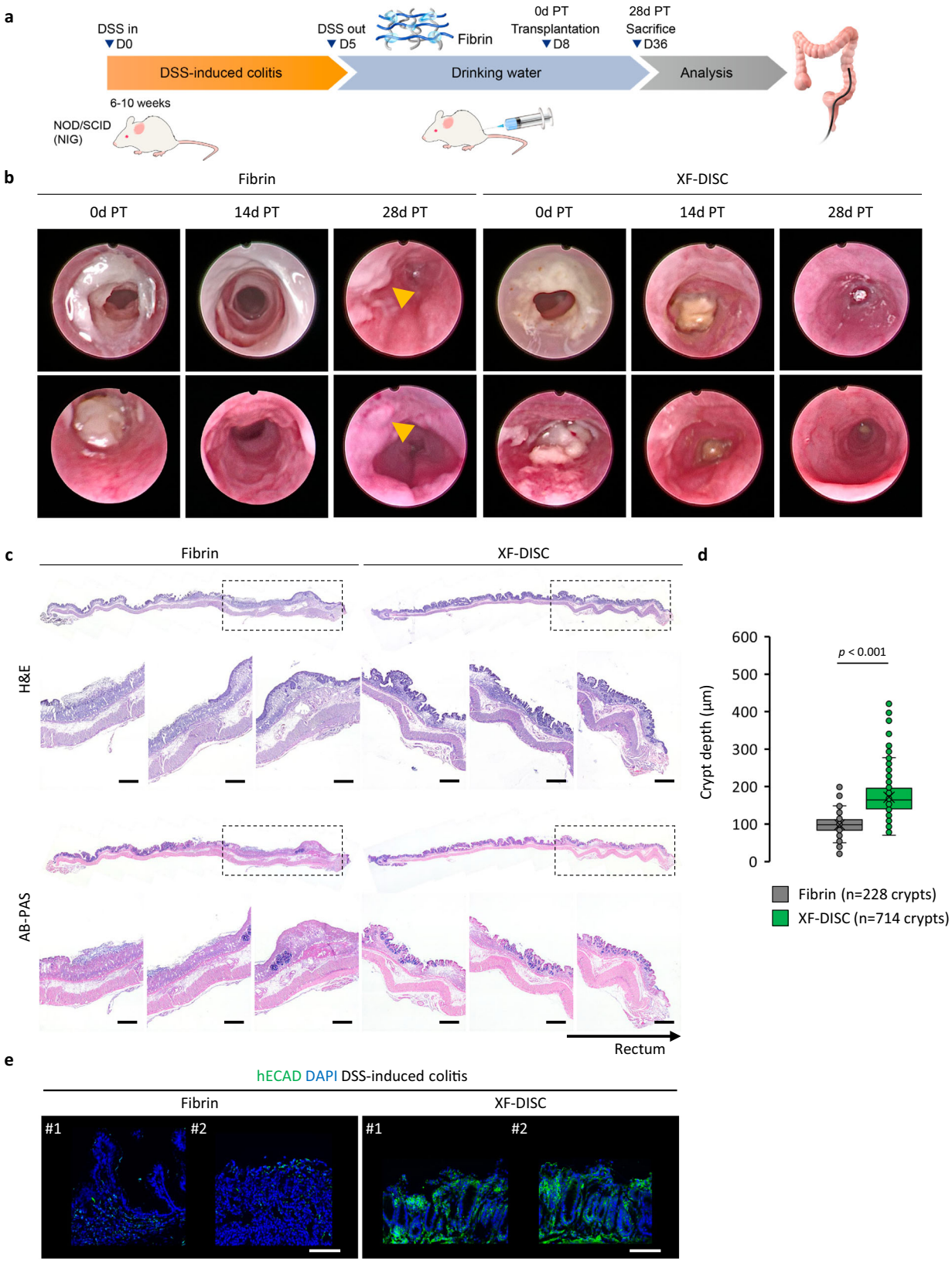

Fig. 7 | Transplantation of ISCs$^{3D\text{-}hIO}$ Cultured on XF-DISCs in DSS-induced Colitis. a Workflow of ISC$^{3D\text{-}hIO}$ transplantation in NOD/SCID mice. **b** Representative mouse colonoscopic observations over time. **c** Top, histopathology of the xenograft colon tissues by H&E staining ($n = 10$ samples/group). Bottom, mucin staining of the xenograft colon tissues by AB–PAS staining. Scale bar: 500 μm ($n = 2$ samples/group). **d** Box and scatterplots of the crypt depth of fibrin-only ($n = 228$ crypts from three mice; 76, 81, and 71 crypts respectively) and ISCs$^{3D\text{-}hIO}$ on XF-DISC ($n = 714$ crypts from six mice; 115, 131, 110, 118, 65, and 175 crypts respectively) treated xenograft colon tissues following H&E staining. The quartiles of the boxplot are mean ± SD, and a Welch's unpaired *t*-test was applied to measure *p*-value. **e** Human E-cadherin staining of xenograft tissues, indicating xenotransplanted ISCs cultured on XF-DISC ($n = 2$ from each group). Scale bar: 100 μm.

that colon-like tissues lacking villus structures and Paneth cells formed after in vivo transplantation of ISCs$^{3D\text{-}hIO}$. Therefore, further mechanistic studies are needed to understand how signals from in vitro culture systems and the in vivo tissue environment impact cellular decision-making in determining cell/tissue types.

A well-known issue with stem cell therapy is the low survival rate of stem cells in vivo posttransplantation, which adversely affects their ability to promote effective tissue regeneration. This results in suboptimal clinical outcomes, such as delayed tissue recovery and an increased risk of complications. Our study addressed this challenge by developing a xenogeneic-free dish for ISC culture (XF-DISC) that enhances ISC culture and viability in mass culture in vitro. The high-purity ISC culture achieved using this method demonstrated successful engraftment and regeneration. Future studies will focus on enhancing the efficiency, durability, and consistency of ISC-based therapies by combining cells to further improve in vivo survival. This approach has the potential to significantly improve clinical outcomes in patients with severe gastrointestinal diseases by overcoming key limitations of current ISC-based therapies.

Methods

Isolation and culture of human intestinal stem cells$^{3D\text{-}hIO}$

The hIOs were differentiated from H9 hESCs (WiCell Research Institute, Madison, WI, USA) and hiPSCs as described previously[62,65]. In this study, we mainly used a hiPSC line that exhibited stable maintenance, pluripotency, and a normal karyotype. hPSCs were differentiated into definitive endoderm (DE) upon treatment with 100 ng/mL activin A (R&D Systems) for 3 days in RPMI 1640 medium (Gibco) supplemented with increasing concentrations of 0%, 0.2%, or 2% fetal bovine serum (FBS; Gibco). DE cells were cultured with RPMI 1640 medium containing 2% FBS, 500 ng/mL FGF4 (Peprotech, organoEZ Cat No. ospr-007, ORGANOIDSCIENCES Co., Ltd.), 500 ng/mL WNT3A (R&D Systems) or 3 μM CHIR99021 (R&D Systems) for 4 days to promote differentiation into 3D hindgut spheroids. The spheroids were embedded in Matrigel and cultured in hIO medium composed of advanced Dulbecco's modified Eagle's medium (DMEM)/F-12 medium (Gibco) containing 1 × B27 (Invitrogen), 500 ng/mL R-Spondin 1 (Peprotech, organoEZ Cat. No. ospr-001, ORGANOIDSCIENCES Co., Ltd.), 100 ng/mL EGF (R&D Systems, organoEZ Cat. No. ospr-011, ORGANOIDSCIENCES Co., Ltd.) and 100 ng/mL Noggin (R&D Systems, organoEZ Cat. No. ospr-003, ORGANOIDSCIENCES Co., Ltd.). To obtain ISCs$^{3D\text{-}hIO}$ from hIOs, hIOs were harvested from the Matrigel dome and digested with trypsin-EDTA for at least 5 min in a 37 °C water bath. The dissociated cells were subsequently harvested and diluted in basal medium composed of advanced DMEM/F12 medium containing 1 × B27, 15 mM HEPES (Gibco), 2 mM L-glutamine (Gibco), and 1% (v/v) penicillin/streptomycin (Gibco). ISCs$^{3D\text{-}hIO}$ were seeded on cell culture dishes at a seeding density of 5×10^4 cells/cm^2 that were coated with 1% Matrigel (Corning, Matrigel Growth Factor Reduced (GFR) Basement Membrane Matrix, LDEV-free, 10 mL, 354230, Lot number: 2271003 J, 2319004) for one hour or XF-DISC. ISCs$^{3D\text{-}hIO}$ were cultured in basal media supplemented with 200 ng/mL R-Spondin 1, 100 ng/mL EGF, 100 ng/mL Noggin, 10 nM [Leu15]-Gastrin 1 (Sigma–Aldrich), 100 ng/m WNT3A, 500 nM A-83-01 (Tocris), 10 μM SB202190 (Sigma–Aldrich), 2.5 μM prostaglandin E_2 (PGE_2) (Sigma–Aldrich), 1 mM N-acetylcysteine (Sigma–Aldrich), and 10 mM nicotinamide (Sigma–Aldrich) at 37 °C in a humidified 5% CO_2 incubator. First, 1 μM Jagged-1 (AnaSpec Inc.) and 2.5 μM Y-27632 (Tocris) were added to the culture medium only after the cells were seeded on the culture dish. The culture media was replaced every 2 days. ISCs were dissociated with TrypLE Express solution (Gibco) for 10 to 15 min at 37 °C and passaged every 7 to 10 days.

Air–liquid interface differentiation of intestinal stem cells$^{3D\text{-}hIO}$

For air–liquid interface (ALI) differentiation of ISCs$^{3D\text{-}hIO}$ into the small intestinal epithelium, Transwell inserts (Corning) were precoated with 5% Matrigel (Corning, Matrigel Growth Factor Reduced (GFR) Basement Membrane Matrix, LDEV-free, 10 mL, 354230, Lot number: 2271003J, 2319004) and incubated at 37 °C for 1 hour or XF-DISC. A total of 250,000–500,000 ISCs were seeded into the apical side of Transwell inserts and cultured with culture medium. At confluency (3–5 days), the apical media was removed, and the small intestinal growth media containing basal media supplemented with 100 ng/mL EGF, 10 μM SB202190, 2.5 μM PGE_2, 200 ng/mL R-Spondin 1, and 10 mM nicotinamide was injected into the basolateral side for ALI differentiation and cultured for an additional 8–12 days before further analysis.

Cell viability assay

ISCs$^{3D\text{-}hIO}$ cultured for 6–7 days were stained with calcein-AM (for live cells) and ethidium homodimer-1 (for dead cells) (LIVE/DEAD Viability/Cytotoxicity Kit, Invitrogen) following the manufacturer's instructions. The cells were subsequently imaged via a fluorescence microscope (Nikon) with NIS-Elements software and analyzed via ImageJ software (NIH) ($n = 3$).

Cell proliferation assay

ISCs$^{3D\text{-}hIO}$ were dissociated and reseeded on 96-well plates. A total of 1×10^4 cells/well were cultured in a culture medium for 5–7 days. The medium was then removed and replaced with 100 μL of fresh medium containing 10 μL of WST-1 cell proliferation reagent (Roche). After incubation for 30–180 min, the absorbance was recorded at 440 nm (reference wavelength, 650 nm) via a microplate reader (Molecular Devices) ($n = 3$).

Crystal violet staining

ISCs$^{3D\text{-}hIO}$ were fixed with 4% paraformaldehyde and stained with 0.02% crystal violet solution (Sigma–Aldrich) at room temperature for 10 min. Next, the samples were washed with water 3 times, and images were captured via the iPhone XS Max (Apple). The colony areas of the ISCs were calculated via ImageJ software (National Institute of Health).

Cell freezing and thawing

To freeze the cells, ISCs$^{3D\text{-}hIO}$ were dissociated with trypsin-EDTA, resuspended in recovery cell culture freezing medium (Gibco) at a density of 2×10^6 cells/mL, and divided into biobanking and cell culture cryogenic tubes (Thermo Scientific). The cell stock vials containing cells were placed in a banking box with isopropyl alcohol (IPA) and frozen at −80 °C for one day before being stored in an LN_2 tank. For the thawing of the cells, the stock vials were thawed at 37 °C for less than 3 min, and the cells were subsequently diluted in basal medium and centrifuged. Then, the cells were resuspended in a culture medium and seeded on culture surfaces at the desired density.

TEER measurement

TEER values were measured via an epithelial tissue volt/ohmmeter (EVOM2, WPI) following the manufacturer's instructions. Briefly, to measure the TEER values of intestinal tissue, two electrodes of the volt/ohmmeter were positioned on the apical and basolateral sides of Transwell inserts. By subtracting the values obtained from inserts without cells, the final TEER values were obtained.

Processing, immunostaining and hematoxylin and eosin (H&E) staining

ALI differentiated samples and xenografts were fixed with 4% paraformaldehyde and frozen in optimal-cutting temperature (OCT) compound (Sakura Finetek). The frozen samples were cut at a thickness of 10–20 μm via a cryostat microtome (Leica) at -20 °C. 2D colony ISCs were fixed with 4% paraformaldehyde solution. For immunofluorescence, the samples were permeabilized with 0.1% Triton X-100 (Sigma–Aldrich) in phosphate-buffered saline (PBS, Welgene) at room

temperature for 10 min. Next, the blocking step was performed with 1% or 4% bovine serum albumin (BSA, Bovogen Biologicals), 22.52 mg/mL glycine (Sigma–Aldrich), and 0.1% Tween 20 (Sigma–Aldrich) in PBS at room temperature for 30 min. The samples were incubated with primary antibodies in 1% BSA and 0.1% Tween 20 in PBS at room temperature for 1 h or at 4 °C overnight. The primary antibodies used in this study are listed in Supplementary Table 6. After washing with PBS, the samples were incubated with DAPI and secondary antibodies (Alexa Fluor 488 donkey anti-goat IgG antibody (Invitrogen), Alexa Fluor 594 donkey anti-mouse IgG antibody (Invitrogen), Alexa Fluor 594 donkey anti-rabbit IgG antibody (Invitrogen), goat anti-mouse IgG Alexa Fluor 488 (Abcam), and goat anti-rabbit IgG Alexa Fluor 594 (Abcam)) with respect to the antigens of primary antibodies diluted in 1% BSA in PBS (1:1000) at room temperature for 1 h and washed with PBS. For H&E staining, samples were stained with hematoxylin and eosin solution (Sigma–Aldrich). All images were obtained via an inverted Eclipse Ti-U series (Nikon) microscope with NIS-Elements software, an IX51 microscope (Olympus, Tokyo, Japan), an EVOS FL Auto 2 (Thermo Fisher Scientific, Waltham, MA, USA) or an LSM 880 confocal microscope (CarlZeiss) with LSM software.

Histopathological analysis

The xenograft colon tissues were fixed with 10% formalin (Sigma–Aldrich, St. Louis, MO, USA) and incubated with 10–30% sucrose serially for cryopreservation. Frozen samples were cut at a thickness of 7–10 μm. For histological analysis, sectioned tissues were stained with H&E. Alcian blue (Abcam, Cambridge, UK)-PAS (Millipore Sigma, Burlington, MA, USA) was used to stain xenograft tissues to identify mucin secretion and goblet cells following the manufacturer's protocol. All images were obtained via a BX53 microscope (Olympus). The colon depth was measured via H&E-stained images via ImageJ software.

Quantitative real-time PCR (qRT–PCR)

RNA was extracted via an RNeasy Kit (Qiagen), and reverse transcription was performed via ReverTra Ace™ qPCR RT Master Mix with gDNA Remover (TOYOBO). qRT–PCR was conducted for triplicate samples via the CFX Connect Optics Module (Bio-Rad) with SYBR qPCR Mix (TOYOBO) according to the manufacturer's instructions. A housekeeping gene encoding glyceraldehyde-3-phosphate dehydrogenase (*GAPDH*) was used as an internal control. The RNA extracted from ISCs cultured on Matrigel-coated surfaces was used as a positive control. The primers used in this study are listed in Supplementary Table 7. The expression levels relative to those of the housekeeping gene (*GAPDH*) were determined via the $2^{-\Delta\Delta Ct}$ method ($n = 3$).

Live cell imaging

The adhesion and colony formation of ISCs on the Matrigel-coated surface and XF-DISC were monitored using an optical microscope (Lumascope 620, Etaluma). Images were captured every 30 s for 12 h after seeding and for 23 h on Days 2 and 7 with a 10× objective lens. The captured images were processed via Adobe premiere Pro 2020 to make Movies.

FACS analysis

The harvested cells were fixed with 4% paraformaldehyde (PFA) for 10 min and permeabilized with 0.1% Triton X-100 (Sigma–Aldrich) in phosphate-buffered saline (PBS, Welgene) at room temperature for 10 min. Next, the blocking step was performed using human fluorochrome block reagent (BD Pharmingen) in FACS buffer consisting of 1% FBS and 0.1% sodium azide (Sigma–Aldrich) in PBS at 4 °C for 10 min, followed by the incubation with primary antibodies in FACS buffer at 4 °C for 10 min. The primary antibodies used in this analysis are listed in Supplementary Table 6. After washing with FACS buffer, the samples were incubated with secondary antibody (Alexa Fluor 488 donkey anti-mouse IgG antibody (Invitrogen)) diluted in FACS buffer (1:1000) at 4 °C for 20 min and washed with PBS. The FACS analysis was obtained using FACSVerse flow cytometry (BD Biosciences).

Endotoxin level assay

The endotoxin level of XF-DISC was assayed via the Pierce™ Chromogenic Endotoxin Quant Kit (Thermo Fisher Scientific) following the manufacturer's procedure. Briefly, endotoxin-free water was added to 96-well cell culture plates containing TCPS and XF-DISC for 24 h. After incubation, the absorbance of the samples was measured at 405 nm via a microplate reader (Molecular Devices), and a standard curve with a coefficient of determination of $r^2 \geq 0.98$ was generated ($n = 3$).

Lymphocyte reaction assay

This study, which was approved by the IRB at Yonsei University Health System (IRB No. 3-2023-0347) aimed to quantify the proliferating CD3-positive T-cell population among peripheral blood mononuclear cells (PBMCs) via FACS analysis. PBMCs were isolated from blood samples and labeled with carboxyfluorescein succinimidyl ester (CFSE; Invitrogen) to monitor cell proliferation. The labeled PBMCs were cultured at a seeding density of 5×10^5 cells/mL for 5 days. After the culture period, the cells were harvested and fixed with 4% PFA for 10 min. The fixed cells were blocked with a human fluorochrome blocker (BD Pharmingen) in FACS buffer and then labeled with a CD3-APC antibody (Cytek) to identify CD3-positive T cells at 4 °C for 20 min. As a positive control, PBMCs were cultured with 5 μg/mL phytohemagglutinin-L (PHA-L). The resulting data from the FACS analysis using FACSVerse flow cytometry enabled the quantification of proliferating CD3-positive T cells. The Gating strategy for CD3-positive T cells is described in Supplementary Fig. 9.

Inflammatory cytokine (TNF-α) assay

Inflammatory cytokine (TNF-α) secretion from RAW 264.7 mouse macrophages (Korean Cell Line Bank) and THP-1 human monocytes (ATCC) cultured on XF-DISC was measured to evaluate immunogenicity via a mouse or human TNF-alpha quantitative ELISA kit (R&D Systems) following the manufacturer's procedure. Briefly, RAW 264.7 macrophages and THP-1 monocytes were cultured at seeding densities of 3.5×10^6 cells/mL and 3×10^6 cells/mL, and the conditioned medium was harvested after 12 h and tested via an ELISA kit. RAW 264.7 macrophages and THP-1 monocytes cultured with 5 μg/mL lipopolysaccharide (LPS) were used as positive controls.

Proteomic analysis

Sodium chloride (NaCl), Tris-HCl buffer (pH 8.0), ammonium bicarbonate (AmBic), dithiothreitol (DTT), iodoacetamide (IAA), L-cysteine, phosphate-buffered saline (PBS), and formic acid (FA) were purchased from Sigma–Aldrich (St. Louis, MO, USA). Protease inhibitor cocktails were obtained from Roche Diagnostic GmbH (Mannheim, Germany). HLB cartridges purchased from Waters (MA, USA) were used. Water (with 0.1% FA), acetonitrile (ACN) (with 0.1% FA), n-dodecyl beta-D-maltoside (DDM), trypsin and bicinchoninic acid (BCA) protein assay reagents were obtained from Thermo Fisher Scientific (Rockford, IL, USA). For proteomic analysis, ISCs cultured for 7 days were harvested after washing with DPBS 3 times and dissociated with TrypLE Express solution ($n = 3$ biological samples). After the cells were harvested, 200 μl of lysis buffer composed of 0.2% DDM, 150 mM NaCl, and one tablet of protease inhibitor cocktail in 50 mM Tris-HCl solution was added to the cell pellets. The mixture was vigorously vortexed for 1 min and then lysed at 95 °C for 10 min in a thermomixer. To remove the cell debris, the mixture was centrifuged at 12,000 × *g* at 4 °C for 15 min, and the supernatant was transferred to a new tube for protein separation. The protein concentrations of the cell lysates were measured via a BCA assay. A total of 20 μg of protein was reduced by adding 50 mM AmBic buffer containing 10 mM DTT at 37 °C for 2 h and then subsequently alkylated with the addition of IAA solution (the final

concentration of IAA was 20 mM) for 30 min at room temperature in the dark. To remove the remaining IAA, L-cysteine was added so that the final concentration was 40 mM, and the mixture was incubated at room temperature for 30 min, followed by tryptic digestion of the samples (enzyme-to-substrate ratio of 1:20). The digestion was performed overnight at 37 °C and quenched with 5% FA. The digests were purified with an HLB cartridge and eluted with 0.5 mL of H2O:ACN (50:50, v/v) solution containing 0.1% FA. After evaporation, the peptides were subjected to nanoflow liquid chromatography–electrospray ionization–tandem mass spectrometry (nanoLC–ESI–MS–MS/MS) analysis. The raw data obtained from the LC–MS/MS data were searched via PEAKS Studio 10.5 (Bioinformatics Solutions, Waterloo, Canada) against the SwissProt database of *Homo sapiens* (human, UP00000564, downloaded 22/11/2019, 20379 entries) from UniProt (http://www.uniprot.org/). The mass error tolerances were set to 20.0 ppm for precursor ions and 0.05 Da for fragment ions. A maximum of two missed cleavages were allowed, and the false discovery rate (FDR) was set to 0.01 for protein identification and label-free quantification (LFQ). The search parameters included a fixed modification of carbamidomethylation of cysteine and variable modifications of oxidation of methionine and acetylation of the protein N-term. Label-free quantification (LFQ) was performed using the analyzed PEAKS file after protein identification was completed. LFQ-based proteomic analysis was performed via ANOVA, and several data filters were set to for LFQ at two or more unique peptides, with at least two samples per group, a minimum p value = 0.01 and a 4.0-fold change. The data were normalized via total ion chromatography. The resulting data were exported to Microsoft Excel, and volcano plots were generated via the Origin program (2019).

RNA sequencing

The RNA samples were analyzed using the Agilent 2100 Bioanalyzer system (Agilent Biotechnologies). Only high-quality RNA samples with an RNA integrity number of ≥ 7.5 were applied for sequencing preparation. Libraries were generated exploiting Illumina TruSeq library preparation, following the instruction of manufacturer. RNA sequencing was conducted on an Illumina HiSeq2500 (Illumina, San Diego, CA, USA) in accordance with the standard Illumina RNA-Seq protocol, using a read length of 2 × 100 bases.

Bioinformatic analysis

The sequence data were evaluated via NGSQCToolkit v.2.3.3, and the adapters were removed via Cutadapt v.1.18 with default settings. Low-quality sequences were trimmed via Sickle v.1.33 with a Phred quality threshold score of 20. If the trimmed read contained any ambiguous character (such as N) or was less than 50 bp, it was excluded. After raw reads were preprocessed, the clean reads were mapped to the reference genome (GRCh38) via HISAT2 v.2.0.5 with default parameter settings, and StringTie v.2.1.0 was applied to the reference annotation file to estimate the expression levels of all genes and transcripts. Using all protein-coding genes, multidimensional scaling (MDS) analysis was performed to cluster the samples according to their overall similarity in terms of gene expression patterns to determine whether the gene expression patterns between the phenotype classes could be clearly distinguished. Here, log2 transformation values were used for the analysis, and rows with zero expression in all samples were eliminated. The MDS analysis of the pairwise distances of the sample was conducted via the function dist (maximum distance measure) in the R v.4.0.2 statistical programming language and plotted via the R package. Adult small intestine RNA-seq data were downloaded from the public database under accession number E-MTAB-1733.

Synthesis of polymers using the iCVD process

The culture plates were loaded in a custom-built iCVD chamber. To deposit the iCVD polymers, the monomers listed in Supplementary Table 1 and *tert*-butyl peroxide (TBPO) (Sigma–Aldrich, 98%) as the initiator were vaporized into the iCVD chamber. The temperature of the filament was set to 140 °C to dissociate the initiator to form radicals. The temperature of the substrate in the chamber, where the culture plates were loaded, was cooled to deposit the polymer. Detailed information on the monomers and deposition conditions for each polymer film is listed in detail in Supplementary Table 2. To enhance the wettability of the polymer surfaces, iCVD polymer-coated dishes were loaded into the chamber of a low-pressure radio frequency (RF) plasma system (Daeki Hi-tech Co., Ltd.) (Supplementary Fig. 10). The chamber pressure was evacuated down to a base pressure lower than 10 mTorr with 5 sccm N_2 gas injection into the chamber. The RF power was set to 15 W, and the plasma treatment time on the polymer surface was set to 10 s.

Polymer film characterization

The water contact angle and glycerol contact angle were measured with a contact angle analyzer (Phoenix 150, Surface Electro Optics, Inc.) by dropping 2 μL droplets of deionized (DI) water. The surface energy was calculated using the Owens, Wednt, Rabel, and Kaelble (OWRK) equation with the contact angle values of two liquids and known disperse and polar parts of surface tension (Eq. 1)[66].

$$\gamma_L(1+\cos\theta) = 2\left\{\left(\gamma_S^P\gamma_L^P\right)^{1/2} + \left(\gamma_S^D\gamma_L^D\right)^{1/2}\right\} \quad (1)$$

γ_L^P and γ_L^D represent the polar and disperse parts of the liquid, respectively, and γ_S^P and γ_S^D represent the polar and dispersive parts of the solid, respectively. θ is the contact angle value of the testing liquid on the polymer surface. Deionized water ($\gamma = 72.8\ mJ\ m^{-2}$, $\gamma^P = 51.0\ mJ\ m^{-2}$, $\gamma^D = 21.8\ mJ\ m^{-2}$) and glycerol ($\gamma = 63.4\ mJ\ m^{-2}$, $\gamma^P = 26.4\ mJ\ m^{-2}$, $\gamma^D = 37.0\ mJ\ m^{-2}$) were used in this study.

The surface morphology of the polymer films was analyzed via atomic force microscopy (AFM), NX-10 (Park Systems). Polymerization of the polymers was confirmed by Fourier transform infrared (FT-IR) spectroscopy performed with an Alpha FT-IR spectrometer (Bruker). The spectra of the polymers were obtained via 64 average scans in absorbance mode at a resolution of 4 cm^{-1} within the range of 4000–400 cm^{-1}. The surface chemical compositions of XF-DISC were analyzed via X-ray photoelectron spectroscopy (XPS) with a K-alpha instrument (Thermo VG Scientific, Inc.).

Xenotransplantation of ISCs$^{3D\text{-}hIO}$ and colonoscopy examination

Male NIG mice (Nod/scid-IL2Rg^{eml}/GH, 6–12 weeks old; GHBio (Daejeon, Korea)) were housed in a specific pathogen-free facility with a controlled 12-hour light/dark cycle, temperature maintained at 20-22 °C, and relative humidity at 55 ± 5%. The mice were provided with ad libitum access to water and fed a purified AIN-76A diet (Teklad Custom Research Diet, CA.170481; Envigo, Indianapolis, IN, USA). The mice were anesthetized via Avertin. The mice were used for a hot EDTA-induced intestinal injury model and a DSS-induced colitis model, as previously described[12,18,67,68]. To remove luminal contents, the mouse colon was flushed with PBS via a flexible catheter. The colon was subsequently filled with 500 μL of 250 mM EDTA/PBS at 50 °C (hot EDTA) and allowed to leak slowly for 2 minutes. After EDTA exposure, epithelial abrasions were created via an electric toothbrush. Approximately 1.5 to 2 cm of the colon surface was gently scratched. Following scratching, the lumen was washed with PBS and observed via colonoscopy. The DSS-induced colitis model was treated with drinking water containing 5% (w/v) DSS (36–50 kDa; MP Biomedicals, Hampton, NH, USA) for 5 days. To remove the DSS contents from the digestive tract, drinking water was provided for 3 days. In the DSS-induced colitis model, body weight, stool consistency, and bleeding parameters were measured daily and confirmed via colonoscopy (Image 1 Hub HD H3-Z; D-Light C; Rigid HOPKINS telescope; Karl Storz, Tuttlingen, Germany; optimized injector; Vetcom, Gwacheon, Korea) on the transplantation

day. For xenotransplantation, $ISCs^{3D\text{-}hIO}$ were dissociated with TrypLE, washed with Advanced DMEM/F12, and suspended in fibrin. One hundred microliters of fibrin suspension contained 1–2 × 10^6 cells. Before transplantation, the recipients were not fasted, were fed a standard diet, and were anesthetized with 250–500 mg/kg tribromoethanol (Avertin) via intraperitoneal injection. A flexible catheter was inserted into the mouse colon, which was subsequently washed with PBS to remove the intestinal contents. Fibrin alone was injected, or $ISCs^{3D\text{-}hIO}$ diluted in fibrin were injected into the colon lumen of intestinal disease model mice via a 200-μL pipette or endoscopic catheter. The recipients were monitored via colonoscopy to track the xenograft colon over time. The mice were euthanized on Days 14 and 28, and the colons and main organs were visually inspected and isolated for analysis. All animal experiments were approved by the Institutional Animal Care and Use Committee (IACUC) of KRIBB (KRIBB-AEC-22233).

Statistics and reproducibility

Origin 2019 and Microsoft Excel 2019 were used for data visualization and analysis. A two-tailed Student's *t*-test and one-way ANOVA followed by Tukey's post hoc test were used to determine the statistical significance of the data, and the results are presented as the mean ± standard deviation (SD). The number of samples and independent biological experimental repeats were indicated in the figures or figure legends. Differences between means of the crypt depth from individual groups were determined using Welch's *t*-test. The significance is depicted as the *p* value.

Reporting summary

Further information on research design is available in the Nature Portfolio Reporting Summary linked to this article.

Data availability

The source data for all figures are provided as a Source Data File with this paper. The bulk RNA-seq data that support the findings of this study has been deposited in Gene Expression Omnibus (GEO) with the accession number GSE261785. The proteomic data in this study has been deposited in ProteomeXchange with the accession number PXD050747. All the data generated and/or analyzed in this study can be found in the published article or the supplementary information files. Any data in this article are available from the corresponding authors (Sung Gap Im; sgim@kaist.ac.kr and Mi-young Son; myson@kribb.re.kr) upon request, and the requests will be fulfilled within 2 weeks. Source data are provided with this paper.

References

1. Wang, Y. et al. Global Burden Of Digestive Diseases: A Systematic Analysis Of the Global Burden of Diseases Study, 1990 to 2019. *Gastroenterology* **165**, 773–783.e715 (2023).
2. Card, T., Hubbard, R. & Logan, R. F. A. Mortality in inflammatory bowel disease: a population-based cohort study. *Gastroenterology* **125**, 1583–1590 (2003).
3. Yang, X. et al. Probiotics-loaded microcapsules from gas-assisted microfluidics for inflammatory bowel disease treatment. *Macromol. Res.* **31**, 817–825 (2023).
4. Kaplan, G. G. & Windsor, J. W. The four epidemiological stages in the global evolution of inflammatory bowel disease. *Nat. Rev. Gastroenterol. Hepatol.* **18**, 56–66 (2021).
5. Sato, T. et al. Single Lgr5 stem cells build crypt-villus structures in vitro without a mesenchymal niche. *Nature* **459**, 262–265 (2009).
6. Fatehullah, A., Tan, S. H. & Barker, N. Organoids as an in vitro model of human development and disease. *Nat. Cell Biol.* **18**, 246–254 (2016).
7. Clevers, H. Modeling development and disease with organoids. *Cell* **165**, 1586–1597 (2016).
8. Sato, T. et al. Paneth cells constitute the niche for Lgr5 stem cells in intestinal crypts. *Nature* **469**, 415–418 (2011).
9. Gjorevski, N. et al. Tissue geometry drives deterministic organoid patterning. *Science* **375**, eaaw9021 (2022).
10. Spence, J. R. et al. Directed differentiation of human pluripotent stem cells into intestinal tissue in vitro. *Nature* **470**, 105–109 (2011).
11. Sugimoto, S. et al. An organoid-based organ-repurposing approach to treat short bowel syndrome. *Nature* **592**, 99–104 (2021).
12. Sugimoto, S. et al. Reconstruction of the human colon epithelium in vivo. *Cell Stem Cell* **22**, 171–176.e175 (2018).
13. Yui, S. R. et al. Functional engraftment of colon epithelium expanded in vitro from a single adult Lgr5(+) stem cell. *Nat. Med* **18**, 618–623 (2012).
14. Watson, C. L. et al. An in vivo model of human small intestine using pluripotent stem cells. *Nat. Med.* **20**, 1310–1314 (2014).
15. Fordham, R. P. et al. Transplantation of expanded fetal intestinal progenitors contributes to colon regeneration after injury. *Cell Stem Cell* **13**, 734–744 (2013).
16. Wang, F. et al. Isolation and characterization of intestinal stem cells based on surface marker combinations and colony-formation assay. *Gastroenterology* **145**, 383–395 (2013).
17. Wang, X. et al. Cloning and variation of ground state intestinal stem cells. *Nature* **522**, 173–178 (2015).
18. Kwon, O. et al. Chemically-defined and scalable culture system for intestinal stem cells derived from human intestinal organoids. *Nat. Commun.* **15**, 799 (2024).
19. Carlson Scholz, J. A. et al. Poliomyelitis in MuLV-infected ICR-SCID mice after injection of basement membrane matrix contaminated with lactate dehydrogenase-elevating virus. *Comp. Med.* **61**, 404–411 (2011).
20. Martin, M. J., Muotri, A., Gage, F. & Varki, A. Human embryonic stem cells express an immunogenic nonhuman sialic acid. *Nat. Med.* **11**, 228–232 (2005).
21. Cruz-Acuna, R. et al. Synthetic hydrogels for human intestinal organoid generation and colonic wound repair. *Nat. Cell Biol.* **19**, 1326 (2017).
22. Yavitt, F. M. et al. The effect of thiol structure on allyl sulfide photodegradable hydrogels and their application as a degradable scaffold for organoid passaging. *Adv. Mater.* **32**, e1905366 (2020).
23. Hernandez-Gordillo, V. et al. Fully synthetic matrices for in vitro culture of primary human intestinal enteroids and endometrial organoids. *Biomaterials* **254**, 120125 (2020).
24. Hunt, D. R. et al. Engineered matrices enable the culture of human patient-derived intestinal organoids. *Adv. Sci.* **8**, 2004705 (2021).
25. Broguiere, N. et al. Growth of epithelial organoids in a defined hydrogel. *Adv. Mater.* **30**, 1801621 (2018).
26. Chrisnandy, A., Blondel, D., Rezakhani, S., Broguiere, N. & Lutolf, M. P. Synthetic dynamic hydrogels promote degradation-independent in vitro organogenesis. *Nat. Mater.* **21**, 479–487 (2022).
27. Petrus-Reurer, S. et al. Immunological considerations and challenges for regenerative cellular therapies. *Commun. Biol.* **4**, 798 (2021).
28. Yu, S. J. et al. Initiated chemical vapor deposition: a versatile tool for various device applications. *Adv. Eng. Mater.* **20**, 31–40 (2018).
29. Baek, J. et al. A surface-tailoring method for rapid non-thermosensitive cell-sheet engineering via functional polymer coatings. *Adv. Mater.* **32**, e1907225 (2020).
30. Choi, Y. et al. Multifunctional printable micropattern array for digital nucleic acid assay for microbial pathogen detection. *ACS Appl Mater. Interfaces* **13**, 3098–3108 (2021).
31. Yu, S. B. et al. Polymer thin films with tunable acetylcholine-like functionality enable long-term culture of primary hippocampal neurons. *ACS Nano* **10**, 9909–9918 (2016).

32. Lee, M. et al. Surface hydrophobicity modulates the key characteristics of cancer spheroids through the interaction with the adsorbed proteins. *Adv. Funct. Mater.* **31**, 2100775 (2021).
33. Park, E. et al. Wettability-based cell sorting: exploring label-free isolation strategy for mixed primary glial cell population. *Adv. Mater. Interfaces* **9**, 2200388 (2022).
34. Choi, G. et al. Antibacterial nanopillar array for an implantable intraocular lens. *Adv. Health. Mater.* **9**, e2000447 (2020).
35. Lee, M. et al. Engineering of surface energy of cell-culture platform to enhance the growth and differentiation of dendritic cells via vapor-phase synthesized functional polymer films. *Small* **18**, 2106648 (2022).
36. Yu, S. J. et al. Three-dimensional spheroid culture on polymer-coated surface potentiate stem cell functions via enhanced cell-extracellular matrix interactions. *ACS Biomater. Sci. Eng.* **6**, 2240–2250 (2020).
37. Park, H. J. et al. Paper-based bioactive scaffolds for stem cell-mediated bone tissue engineering. *Biomaterials* **35**, 9811–9823 (2014).
38. Hoshiba, T., Yoshikawa, C. & Sakakibara, K. Characterization of initial cell adhesion on charged polymer substrates in serum-containing and serum-free media. *Langmuir* **34**, 4043–4051 (2018).
39. Kim, M. J. et al. BMP-2 peptide-functionalized nanopatterned substrates for enhanced osteogenic differentiation of human mesenchymal stem cells. *Biomaterials* **34**, 7236–7246 (2013).
40. Lee, S. J. et al. Biofunctionalized titanium with anti-fouling resistance by grafting thermo-responsive polymer brushes for the prevention of peri-implantitis. *J. Mater. Chem. B* **3**, 5161–5165 (2015).
41. Youn, Y. H. et al. Simple and facile preparation of recombinant human bone morphogenetic protein-2 immobilized titanium implant via initiated chemical vapor deposition technique to promote osteogenesis for bone tissue engineering application. *Mater. Sci. Eng. C. Mater. Biol. Appl.* **100**, 949–958 (2019).
42. Chung, J. H., Ma, S. Y., Bail, R. & Lee, D. H. Synthesis of crosslinkable polyetherimide and application as an additive in 3D printing of photopolymers. *Macromol. Res.* **30**, 43–50 (2022).
43. Cho, Y., Baek, J., Lee, E. & Im, S. G. Heparin-mediated electrostatic immobilization of bFGF via functional polymer films for enhanced self-renewal of human neural stem cells. *J. Mater. Chem. B* **9**, 2084–2091 (2021).
44. Kwak, M. J. et al. A sub-minute curable nanoadhesive with high transparency, strong adhesion, and excellent flexibility. *Macromolecules* **51**, 992–1001 (2018).
45. Choi, G. et al. Polymer-coated surface as an enzyme-free culture platform to improve human mesenchymal Stem Cell (hMSC) characteristics in extended passaging. *ACS Appl. Bio Mater.* **3**, 7654–7665 (2020).
46. Burke, G. et al. Evaluation of the materials properties, stability and cell response of a range of PEGDMA hydrogels for tissue engineering applications. *J. Mech. Behav. Biomed. Mater.* **99**, 1–10 (2019).
47. Christian, P. et al. Controlling Indomethacin release through vapor-phase deposited hydrogel films by adjusting the cross-linker density. *Sci. Rep.* **8**, 7134 (2018).
48. Sato, T., Ishida, Y. & Kameyama, A. RAFT homopolymerization of vinylbenzyl chloride with benzyl ethyl trithiocarbonate and synthesis of block copolymers from poly(VBC) macro-RAFT agent and N-isopropylacrylamide. *Polym. J.* **46**, 239–242 (2013).
49. Joo, M. et al. One-Step Synthesis Of Cross-linked Ionic Polymer Thin Films In Vapor Phase And Its Application To An Oil/water Separation Membrane. *J. Am. Chem. Soc.* **139**, 2329–2337 (2017).
50. Choi, G. et al. Robust Thin Film Surface With A Selective Antibacterial Property Enabled Via A Cross-linked Ionic Polymer Coating For Infection-resistant Medical Applications. *ACS Biomater. Sci. Eng.* **4**, 2614–2622 (2018).
51. Choi, M. et al. Polymer thin film–induced tumor spheroids acquire cancer stem cell–like properties. *Cancer Res.* **78**, 6890–6902 (2018).
52. Matsuzaka, N., Takahashi, H., Nakayama, M., Kikuchi, A. & Okano, T. Effect of the hydrophobic basal layer of thermoresponsive block co-polymer brushes on thermally-induced cell sheet harvest. *J. Biomater. Sci. Polym. Ed.* **23**, 1301–1314 (2012).
53. Dewez, J. L. et al. Adhesion of mammalian cells to polymer surfaces: from physical chemistry of surfaces to selective adhesion on defined patterns. *Biomaterials* **19**, 1441–1445 (1998).
54. Chai, J., Lu, F., Li, B. & Kwok, D. Y. Wettability interpretation of oxygen plasma modified poly(methyl methacrylate). *Langmuir* **20**, 10919–10927 (2004).
55. Liu, W. et al. Effects of plasma treatment to nanofibers on initial cell adhesion and cell morphology. *Colloids Surf. B Biointerfaces* **113**, 101–106 (2014).
56. Majhy, B., Priyadarshini, P. & Sen, A. K. Effect of surface energy and roughness on cell adhesion and growth - facile surface modification for enhanced cell culture. *RSC Adv.* **11**, 15467–15476 (2021).
57. Owens, D. K. & Wendt, R. C. Estimation of the surface free energy of polymers. *J. Appl. Polym. Sci.* **13**, 1741–1747 (1969).
58. Cequier, A. et al. Equine mesenchymal stem cells influence the proliferative response of lymphocytes: effect of inflammation, differentiation and MHC-compatibility. *Animals* **12**, 984 (2022).
59. Kim, S. et al. Tissue extracellular matrix hydrogels as alternatives to Matrigel for culturing gastrointestinal organoids. *Nat. Commun.* **13**, 1692 (2022).
60. Vargas-Hernandez, O. et al. THP-1 cells increase TNF-alpha production upon LPS + soluble human IgG co-stimulation supporting evidence for TLR4 and Fcgamma receptors crosstalk. *Cell Immunol.* **355**, 104146 (2020).
61. Islam, M. M. et al. Biomaterials-enabled cornea regeneration in patients at high risk for rejection of donor tissue transplantation. *NPJ Regen. Med.* **3**, 2 (2018).
62. Kwon, O. et al. The development of a functional human small intestinal epithelium model for drug absorption. *Sci. Adv.* **7**, eabh1586 (2021).
63. Cruz-Acuna, R. et al. PEG-4MAL hydrogels for human organoid generation, culture, and in vivo delivery. *Nat. Protoc.* **13**, 2102–2119 (2018).
64. Glorevski, N. et al. Designer matrices for intestinal stem cell and organoid culture. *Nature* **539**, 560 (2016).
65. Jung, K. B. et al. Interleukin-2 induces the in vitro maturation of human pluripotent stem cell-derived intestinal organoids. *Nat. Commun.* **9**, 3039 (2018).
66. Kaelble, D. H. Dispersion-polar surface tension properties of organic solids. *J. Adhes.* **2**, 66–81 (1970).
67. Watanabe, S. et al. Transplantation of intestinal organoids into a mouse model of colitis. *Nat. Protoc.* **17**, 649–671 (2022).
68. Dieleman, L. A. et al. Dextran sulfate sodium-induced colitis occurs in severe combined immunodeficient mice. *Gastroenterology* **107**, 1643–1652 (1994).

Acknowledgements

This study was supported by a National Research Foundation of Korea (NRF) grant funded by the Korean Government (MSIP) (no. 2021R1A2B5B03001416, NRF-2018M3A9H3023077/2021M3A9H3016046), a Korean Fund for Regenerative Medicine (KFRM) grant funded by the Korean government (Ministry of Science and ICT, Ministry of Health & Welfare, 21A0404L1) and a grant from the Technology Innovation Program (no. 20008777) funded by the Ministry of Trade, Industry & Energy (MOTIE, Korea), and the KRIBB Research Initiative Program (KGM4722432).

Author contributions

SE.P., O.K. and H.L. contributed equally to this work. SE.P., O.K., H.L., M.-Y.S. and S.G.I. designed the research. SE.P., O.K., H.L., Y.C., J.Y., S.H.Y., S.Y.S., Y.H., W.D.Y., SO.P., N.S., S.J., S.L., D.-S.K., S.Y.L., J.G.S., K.J.L., Y.I.K., J.H.L., J.Y. and T.G.L. performed the experiments. All the authors were involved in the data analysis. SE.P., O.K. and H.L. wrote the manuscript, and all authors discussed and commented on it. M.-Y.S. and S.G.I. directed the research.

Competing interests

The authors declare no competing interests.

Ethical considerations of working with human cells and animals

This study complies with all relevant ethical regulations. All studies based on human pluripotent stem cells were approved by the Korean Public IRB (IRB number: P01-201409-ES-01-09, P01-201609-31-002). Male NIG mice (Nod/scid-IL2Rg^{em1}/GH, 6–12 weeks old; GHBio, Daejeon, Korea) were housed in a specific pathogen-free facility with a controlled 12-hour light/dark cycle, temperature maintained at 20-22 °C, and relative humidity at 55 ± 5%. The mice were provided with ad libitum access to water and fed a purified AIN-76A diet (Teklad Custom Research Diet, CA.170481; Envigo, Indianapolis, IN, USA). All animal experiments were approved by the Institutional Animal Care and Use Committee (IACUC) of KRIBB (KRIBB-AEC-22233). For the study based on human blood, informed consent was obtained prior to participation with approval from the IRB at Yonsei University Health System (IRB No. 3-2023-0347).

Additional information

Supplementary information The online version contains supplementary material available at https://doi.org/10.1038/s41467-024-54653-9.

Correspondence and requests for materials should be addressed to Mi-Young Son or Sung Gap Im.

Peer review information *Nature Communications* thanks David Stresser, who co-reviewed with Sarah Wilson, Shiro Yui, and the other, anonymous, reviewer(s) for their contribution to the peer review of this work. A peer review file is available.

[1]Department of Chemical and Biomolecular Engineering, Korea Advanced Institute of Science and Technology (KAIST), 291 Daehak-ro, Yuseong-gu, Daejeon, Republic of Korea. [2]Stem Cell Convergence Research Center, Korea Research Institute of Bioscience and Biotechnology (KRIBB), 125 Gwahak-ro, Yuseong-gu, Daejeon, Republic of Korea. [3]KRIBB School of Bioscience, Korea University of Science and Technology (UST), Daejeon, Republic of Korea. [4]Digital Biotech Innovation Center, KRIBB, Daejeon, Republic of Korea. [5]Nanobio Measurement Group, Division of Biomedical Metrology, Korea Research Institute of Standards and Science (KRISS), 267 Gajeong-ro, Yuseong-gu, Daejeon, Republic of Korea. [6]R&D Institute, ORGANOIDSCIENCES Ltd., Seongnam, Republic of Korea. [7]Department of Surgery, Gangnam Severance Hospital, Pancreatobiliary Cancer Clinic, Yonsei University College of Medicine, Seoul, Republic of Korea. [8]Organoid Standards Initiative (OSI), Department of Biophysics, Institute of Quantum Biophysics, Sungkyunkwan University, Suwon, Republic of Korea. [9]CHA Organoid Research Center, CHA University, Seongnam, Republic of Korea. [10]School of Medicine, Sungkyunkwan University, Suwon, Republic of Korea. [11]KAIST Stem Cell Center, Department of Chemical and Biomolecular Engineering, Graduate School of Stem Cell & Regenerative Biology, KAIST, Daejeon, Republic of Korea. [12]Present address: KRIBB School of Bioscience, Korea University of Science and Technology (UST), Daejeon, Republic of Korea. [13]These authors contributed equally: Seonghyeon Park, Ohman Kwon, Hana Lee. ✉e-mail: myson@kribb.re.kr; sgim@kaist.ac.kr